JOURNAL
OF THE AMERICAN CHEMICAL SOCIETY

VOLUME 101, NUMBER 16 AUGUST 1, 1979

Binding of Oxygen and Carbon Monoxide to Hemoglobin. An Analysis of the Ground and Excited States

D. A. Case,[1a] B. H. Huynh,[1b] and M. Karplus*

Contribution from the Department of Chemistry, Harvard University, Cambridge, Massachusetts 02138. *Received May 4, 1978*

Abstract: Two quantum mechanical calculations on iron–porphyrin complexes that are models for the active site in oxy- and carboxyhemoglobin are reported. The first calculation uses an extended Pariser–Parr–Pople (PPP) Hamiltonian and includes configuration interaction among singly and doubly excited configurations; the second employs the Xα multiple scattering method. A critical comparison is made between the results of these methods and others (extended Hückel, ab initio Hartree–Fock) that have been used to examine such complexes. Ground-state properties, including the energy and charge distribution, are examined. It is found that correlation effects involving doubly excited configurations must be included to obtain a singlet ground state for the oxygen complex; there is only a small effect from these added configurations on the ground-state charge distribution. The FeO_2 unit is shown to be well represented as an equal mixture of $Fe^{2+}(S = 0)$, $O_2(S = 0)$ and $Fe^{2+}(S = 1)$, $O_2(S = 1)$ valence-state pairs; the latter resembles ozone in certain respects. The FeCO unit corresponds closely to an idealized $Fe^{2+}(S = 0)$, $CO(S = 0)$ species. Calculated Mössbauer splittings and infrared stretching frequencies in approximate agreement with the experimental values for both complexes provide support for the present treatment. A detailed analysis of the excited states is presented, and the results are compared with the available data for ten transitions in oxyhemoglobin and five in carboxyhemoglobin. For oxyhemoglobin, in addition to the well-known porphyrin $\pi \rightarrow \pi^*$ transitions, iron d→d transitions and a variety of charge-transfer transitions are identified. Extended Hückel, PPP, and Xα calculations agree that an unoccupied FeO_2 π^* orbital plays an important role in the low-energy spectrum. In carboxyhemoglobin no such low-lying orbital is present and a much simpler spectrum results.

I. Introduction

Hemoglobin and myoglobin are proteins whose heme prosthetic group reversibly binds molecular oxygen. The nature of the bond between iron and oxygen has been a controversial problem for many years, and there remain unanswered questions concerning the details of the electronic structure.[2] It has been found useful to make comparisons between oxygen and carbon monoxide, since the latter can also bind reversibly to hemoglobin. In this paper we present quantum mechanical calculations of the ground and excited states of oxy- and carboxyhemoglobin to develop a framework for discussing the available structural and spectral data. We apply the extended PPP and Xα multiple scattering methods to a model complex consisting of a planar iron porphin with an imidazole group and dioxygen or carbon monoxide as axial ligands. The results of the calculations make possible a detailed description of the ground and low-lying excited states of these systems. Comparisons are made with a variety of experimental results; these include Mössbauer[3] and infrared[4] data which probe the electronic ground state and spectral studies of the excited states. Among the latter, particular emphasis is given to recent measurements and extensive analyses of the optical transitions in oxy- and carboxyhemoglobin[5] and in oxy- and carboxymyoglobin.[6]

Since the many-electron system under consideration is rather complicated it is useful to introduce simplified models for its electronic structure. These are conveniently based on suitable reference configurations. As we discussed earlier[2] the reference states that seem most appropriate for the ground state of oxyhemoglobin arise from the interaction of an iron–porphyrin moiety and an O_2 molecule with both species in either $S = 0$ or $S = 1$ valence states. In the $(S = 0, S = 0)$ model, the iron is ferrous low spin (t_{2g}^6) while the oxygen molecule resides in a spin-paired singlet configuration analogous to that in the $^1\Delta_g$ molecular state; the spin pairing in oxygen occurs because the π_g orbital in the FeO_2 plane has a lower energy than its out-of-plane partner. This reference state corresponds to the original Pauling model,[7] and predicts oxyhemoglobin to be diamagnetic. For the CO adduct, no spin pairing is needed, since the free ligand is already in a closed-shell configuration. Our calculations indicate that the $(S = 0, S = 0)$ reference state is an excellent model for heme–CO, but that there are significant deviations in heme–O_2.

A second reference configuration has both iron and oxygen in $S = 1$ states. The iron is in an excited ferrous state in which one electron has been removed from the d_{xz} orbital (which is antisymmetric with respect to the FeO_2 plane in our coordinate system) and placed into the d_{z^2} orbital (which points along the Fe–O bond); the oxygen retains its $^3\Sigma_g$ configuration. The resulting complex is again diamagnetic owing to the pairing of the two $S = 1$ states. This description corresponds to the idealized ozone model of Goddard and Olafson.[8] Although the resulting populations are not identical with the ones we cal-

0002-7863/79/1501-4433$01.00/0

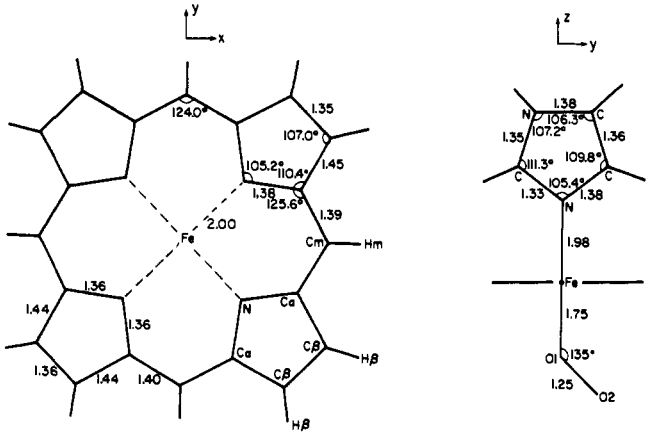

Figure 1. Assumed heme-O_2 geometry. Bond lengths are given in angstroms. Values in the lower left of the porphyrin skeleton are estimated from the PPP bond orders, as discussed in the text.

culated, there do exist many similarities between ozone and heme-O_2. Thus it is useful to discuss heme-O_2 in terms of deviations from the idealized ozone model.

There is a third reference state that is often thought to represent well many experimental features of oxyhemoglobin. This is the Weiss model[9] in which an electron is transferred from iron to dioxygen and the complex consists of a low-spin ferric ion (t_{2g}^5,^{2}E) coordinated to a superoxide anion ($^2\Pi_g$). The diamagnetism of heme-O_2 is presumed to be due to spin pairing of the two doublet configurations. Our calculations show no evidence for such charge transfer in the ground state, although there exists a triplet-singlet pair of excited states of the Weiss type at about 1 eV. It has been pointed out by a number of workers that certain experimental observations appear to support the Weiss description. We have discussed some of this in our earlier communication.[2] In this paper we present in more detail our reasons for believing that the experimental evidence in favor of the Weiss model is not compelling and that the available data are consistent with the model proposed here.

An understanding of the heme-O_2 and heme-CO electronic structure is also required for an analysis of the electronically excited states, whose nature is crucial to the interpretation of spectroscopic studies of mutant hemoglobins or hemoglobins with allosteric effectors such as phosphates.[10,11] Oxyhemoglobin, for example, has a characteristic broad near-infrared transition that has been known for many years;[12] recent single-crystal and magnetic circular dichroism[5] studies have revealed that this band in fact has two components. Other previously unknown transitions have also been characterized.[5,6] It thus becomes a challenging task to predict and assign the low-energy transitions of these two compounds. Furthermore, a consistent explanation provides a posteriori confirmation of our model of the ground state. In this paper we present excitation energies calculated with the transition-state method in the Xα framework, and with extensive configuration interaction in the extended PPP model. It is shown that correlation effects are important for an accurate representation of the excited states; indeed, the very existence of a diamagnetic ground state is found to be dependent upon electron correlation. Thus a detailed interpretation of the electronic spectrum requires judicious use of the molecular orbital picture supplemented where necessary by the introduction of correlation corrections.

As a starting point for quantum-mechanical calculations, it is important to have available the molecular geometry. For FeO_2 and FeCO in myoglobin and hemoglobin the exact structure is not known. However, recent X-ray studies on model oxygen complexes[13] strongly support the bent Fe-O^1-O^2 structure originally proposed by Pauling;[7] further, a preliminary report[14] of a high-resolution X-ray structure of MbO_2, published after completion of our work, is in accord with the Pauling geometry. It is this geometry that we are concerned with here. For the carbon monoxide complex, the linear geometry is an intrinsically favored one, as demonstrated by model studies,[15] but neutron diffraction and X-ray studies on carboxymyoglobin and hemoglobin indicated that the oxygen atom is displaced from the normal to the heme plane.[16,17] It appears likely that the Fe-C-O unit remains linear and is tilted from the normal direction;[17,18] our results for the CO complex refer to the collinear geometry of the model compound. From the similarity between the experimental spectra of model compounds and heme proteins, it is likely that the ground- and excited-state properties considered here are not very sensitive to the exact structures (e.g., iron slightly out of plane) and that the model geometries being used are adequate.

In section II we give the details of the calculations; section III discusses our results for the ground-state properties of heme-O_2 and heme-CO; section IV reviews recent spectroscopic studies on these complexes and compares them with our theoretical results for the excited states.

II. Details of the Calculations

We have performed two types of quantum-mechanical calculations, each with its own advantages and disadvantages. One is of the extended Pariser-Parr-Pople (PPP) type, while the other employs the Xα multiple scattering method. In this section we first present the molecular geometry and then outline the essentials of the two calculational methods.

A. Molecular Geometry. Our model for the active site in oxyhemoglobin consists of an iron atom coordinated in the equatorial plane to the four nitrogens of porphyrin; the axial ligands are O_2 and imidazole (to represent the side chain of histidine F8). The geometry is based on the model compound results of Collman et al.,[13] but we have reduced the distance from iron to the nitrogen of the imidazole ring from 2.07 to 1.98 Å to correspond with fluorescent X-ray absorption results on hemoglobin.[19] This geometry is shown in Figure 1, which also gives bond lengths and angles. The plane of the Fe-O_2 unit and the imidazole ring is taken to be the yz plane, which bisects the N-Fe-N angles connecting iron to the porphyrin. This assumption simplified the calculation but is not in general valid for heme proteins; for MbO_2, the recent X-ray work of Phillips[14] shows that the Fe-O_2 unit and imidazole ring are approximately coplanar and nearly eclipse one of the Fe-N bonds. The iron atom is assumed to be in the plane of the porphyrin. The complex has C_s symmetry; coordinates for the unique atoms are given in Table I. Our axis system is identical with that of Eaton et al.[5]

The geometry of the CO adduct was modeled after a recent X-ray study of Peng and Ibers.[15] Here the Fe-C-O unit is linear and normal to the heme plane (see Table I). The porphine imidazole structure is assumed to be the same as in the oxygen complex.

B. Extended PPP Calculations. The porphyrin ligand forms a macrocyclic conjugated π system that should be well suited to traditional π-electron methods. Indeed, the first convincing calculations on the origin of the visible and Soret bands in heme proteins used a PPP model.[20] An extension of this method to handle transition-metal complexes[21] forms the basis for the present calculations. It takes into account all of the orbitals of primary importance, including the nitrogen lone pairs of porphyrin and imidazole, the iron 3d, 4s, and 4p orbitals, the oxygen and carbon 2s and 2p orbitals, and the π orbitals of porphyrin and imidazole. This makes a total of 51 basis orbitals to represent 60 valence electrons in heme-O_2 and 58 electrons in heme-CO.

Table I. Coordinates of the Unique Atoms (Å)

atom	*x*	*y*	*z*
		Porphine	
Fe	0.0	0.0	0.0
N	1.414	1.414	0.0
Cα	1.231	2.786	0.0
Cβ	2.508	3.465	0.0
Hβ	2.666	4.533	0.0
Cm	0.0	3.441	0.0
Hm	0.0	4.521	0.0
		Imidazole	
N1	0.0	−0.686	4.084
H1	0.0	−1.291	4.905
C2	0.0	−1.058	2.786
H2	0.0	−2.083	2.445
N3	0.0	0.0	1.980
C4	0.0	1.098	2.816
H4	0.0	2.127	2.490
C5	0.0	0.689	4.113
H5	0.0	1.337	4.977
		Oxygen	
O1	0.0	0.0	−1.750
O2	0.0	0.868	−2.649
		Carbon Monoxide	
C	0.0	0.0	−1.770
O	0.0	0.0	−2.890

A Hartree–Fock SCF calculation is done with a Fock matrix of the form

$$F_{\mu\nu} = H_{\mu\nu} + \sum_{\lambda\sigma} P_{\lambda\sigma}[(\mu\nu|\lambda\sigma) - \tfrac{1}{2}(\mu\lambda|\nu\sigma)] \qquad (1)$$

where $\mu\nu\lambda\sigma$ represent atomic orbitals, $P_{\lambda\sigma}$ is the density matrix, $(\mu\nu|\lambda\sigma)$ is a two-electron integral, and $H_{\mu\nu}$ is the matrix of the core Hamiltonian. In calculating the two-electron integrals zero differential overlap is assumed except for the one-center exchange integrals (see Appendix). To calculate the one-electron integrals we employ the approximation

$$H_{\mu\nu} = \langle\mu|H_{\text{core}}|\nu\rangle = \alpha_\mu\delta_{\mu\nu} + \beta_{\mu\nu} \qquad (2)$$

where α_μ is the core integral. The resonance integral $\beta_{\mu\nu}$ is assumed to be nonzero if and only if orbitals ϕ_μ and ϕ_ν belong to neighboring atoms. The core integral $\alpha_\mu^{(i)}$ of orbital ϕ_μ of the ith atom can be written as

$$\alpha_\mu^{(i)} = \langle\mu|T + V_{\text{core}}^{(i)}|\mu\rangle + \sum_{j\neq i} V_{j\mu} \qquad (3)$$

where T is the kinetic energy operator, $V_{\text{core}}^{(i)}$ is the core potential of atom i, and $V_{j\mu}$ represents the attraction between the core of atom j and the electrons in occupied orbital ϕ_μ. The first term of eq 3 can be estimated from atomic spectral data together with the ionization potential. The potential energy $V_{j\mu}$ is approximated by the Goeppert-Mayer–Sklar formula:[22]

$$V_{j\mu} = (\mu|V_j|\mu) - \sum_{\mu}^{(j)} n_\nu\gamma_{\mu\nu} \qquad (4)$$

where n_ν is the total number of electrons explicitly included in the calculations that are associated with the atomic orbital ϕ_ν of atom j, $\gamma_{\mu\nu}$ is the Coulomb repulsion integral for the orbitals ϕ_μ and ϕ_ν, and V_j is the potential of a neutral atom j; the quantity $(\mu|V_j|\mu)$ is called the penetration integral.

We present in the Appendix our values for the required empirical parameters and discuss in more detail the way in which the one- and two-electron integrals are approximated.

With the resulting SCF orbitals, configuration interaction (CI) calculations were made for the ground and excited states.

Table II. Xα Exchange Factors and Sphere Radii

atom	α	*b*/au
Fe	0.711 51	2.62
C	0.753 31	1.60
N	0.745 52	1.60
H	0.776 27	0.95
O	0.741 18	1.50
C[a]	0.753 31	1.50
O[a]	0.751 18	1.40

[a] Values for CO in heme–CO.

Complete single CI calculations and limited single plus double CI calculations were performed. For heme–O_2 there are 30 occupied and 21 unoccupied molecular orbitals. The total number of single excitations of singlet spin symmetry is 630; use of spatial symmetry yields 317 for the A′ representation and 313 for A″. Evaluation and diagonalization of such a Hamiltonian matrix required 12 min on an IBM 360/91.

Unfortunately, the number of configurations increases drastically when higher excitations are included. There are nearly 200 000 double-excited singlet configurations for heme–O_2. Hence a method to choose the important configurations for the double CI is necessary. Selection of these was carried out in two steps.[23] First there was preselection of reference configurations (RCFs) for the states of interest, and second the additional configurations that may be expected to contribute most strongly to the final CI eigenvectors were chosen.

The reference configurations were taken to be the SCF state plus all of the configurations created by single excitation within a certain subset of 20 MOs. This subset was chosen to generate configurations important to excited states up through the Soret region; members of this subset are marked with an asterisk in Tables III and IV. The double-excited configurations (DCFs) generated from these MOs were divided into groups of 65. The importance of each DCF was then estimated by performing separate CI calculations with the RCFs and each group of DCFs. In practice, any DCF appearing in a low-lying eigenvector with a coefficient larger than 0.025 is classified as significant. A final $S + D$ CI calculation was then performed with the RCFs and the 400 selected DCFs. The entire limited double CI calculation required 25 min of computer time.

C. Xα Multiple Scattering Calculations. The Xα multiple scattering method generates an approximate Hartree–Fock molecular wave function. The nonlocal exchange interaction is replaced by a local term, as in the Thomas–Fermi–Dirac model. This approximation and additional ones involving the muffin-tin potential, including overlapping spheres, have been described in several reviews.[24,25] In particular, the work reported here is completely analogous to our previous studies of copper porphin,[26] where we discussed the rationale behind the calculations in some detail. Consequently, we outline only the aspects not covered in the earlier paper.

There are two sets of parameters, in addition to the geometry, that must be specified in the muffin-tin model. The first is the set of exchange parameters, which are almost always taken from atomic calculations;[25] values are given in Table II. The second is the set of cellular radii surrounding each atom. We considered this point in some detail earlier,[26] and the same radii as were employed for copper porphin are used in this study for the porphyrin, the central metal, and the imidazole ring (see Table II). Oxygen and carbon monoxide as ligands have very short internuclear separations (2.38 and 2.12 au, respectively), and this suggests that smaller radii may be necessary for these atoms. Since previous studies have shown that deleterious effects set in for sphere overlaps greater than about 40% (K. H. Johnson, personal communication) we have used radii small

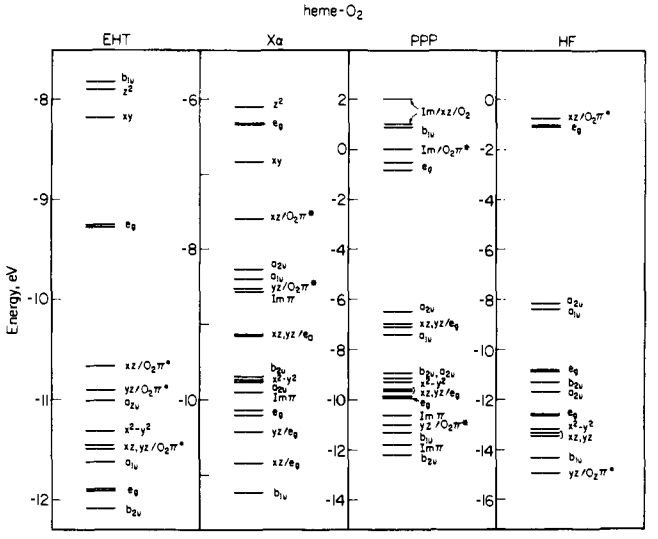

Figure 2. Molecular orbital energies for heme-O_2. Extended Hückel (EHT) results from ref 5; Hartree-Fock (HF) results from ref 35.

enough to avoid this problem. Our percentage overlap for heme-O_2 (26%) is very close to that used by Norman[27] in platinum dioxygen compounds (27%); the latter value was chosen by a determinate, but somewhat arbitrary, algorithm that has given good results for a variety of molecules.[27] The method yields values of 1.49 and 1.45 au for the carbon and oxygen sphere radii in $Cr(CO)_6$;[28] these are close to the values of 1.50 and 1.40 au used in the present study (Table II). It has been shown that such radii yield good results for the ionization potentials of an isolated CO molecule, and that even rather large changes in the radii (±0.2 au) have only a minor effect.[29] The virial ratio, $-V/T$, is sometimes used as a criterion for the appropriateness of sphere radii;[27] our values are 1.986 for both the CO and O_2 complexes.

Once the radii are chosen, self-consistent solutions are generated using standard algorithms.[24] The iterative process was continued until the one-electron energies were converged to 5×10^{-3} eV. This required about 15–20 iterations, with each one requiring 9 min in double precision on an IBM 360/91 computer. One-electron properties were determined by a method described previously.[30] Spin restricted excitation energies were estimated by the Slater transition-state method.[25,31]

III. Ground-State Properties

In this section we present results for the charge distribution, bond orders, molecular orbital structure, and electric field gradients for the ground states of heme-O_2 and heme-CO.

A. Molecular Orbitals. Figure 2 gives the molecular orbital energies for heme-O_2 determined from four different approximate methods. The left-hand column gives extended Hückel results of Eaton et al.,[5] who used the parameters of Zerner, Gouterman, and Kobayashi;[32] similar results have been obtained by Kirchner and Loew,[33] who examined the effect of geometry on the electronic structure of the heme-O_2 complex. A self-consistent charge iteration was used in these calculations[32] in that the atomic ionization potentials are assumed to be a function of the atomic populations. In spite of its approximate nature, this method has proved useful as an interpretative tool and has been applied to a large number of metalloporphyrin complexes.[34] The right-hand column in Figure 2 gives near minimum basis set ab initio Hartree-Fock results of Dedieu, Rohmer, and Veillard.[35] In this calculation an NH_3 group takes the place of imidazole, but otherwise the geometry is nearly identical with the other calculations shown. The two center columns represent the present work. Although each calculation assumed only C_s symmetry, we have labeled the porphyrin orbitals by the representations in D_{4h} from which they are descended.

A striking feature of the diagram is the large difference in energy spacings among the orbitals in the various calculations. Before considering the differences in detail, it is useful to review the meanings of the one-electron energies; this permits us to demonstrate why they are expected to have values that depend strongly on the method of calculation. The best approach is to compare the one-electron energy differences with state energy differences, which are the observables of a spectroscopic experiment. We consider, as an example, a $\pi \rightarrow \pi^*$ transition in the porphyrin ligands. This is a one-electron excitation from a closed shell, so that in the Hartree-Fock approximation the excitation energies for the singlet and triplet states are

$$^1\Delta E = \epsilon_{\pi^*} - \epsilon_{\pi} - J_{\pi\pi^*} + 2K_{\pi\pi^*} \qquad (5)$$

$$^3\Delta E = \epsilon_{\pi^*} - \epsilon_{\pi} - J_{\pi\pi^*}$$

and the average of these is

$$\Delta E = \epsilon_{\pi^*} - \epsilon_{\pi} - J_{\pi\pi^*} + K_{\pi\pi^*} \qquad (6)$$

Since the Coulomb integrals are much larger than the exchange integrals, the one-electron energy difference must be larger than the average state energy difference. For the PPP calculation, typically $J_{\pi\pi^*} \approx 4.5$ eV while $K_{\pi\pi^*} \approx 0.5$ eV. The difference $\epsilon_{\pi^*} - \epsilon_{\pi}$ between the top π and bottom π^* orbital is about 6 eV (see Figure 2). Hence $\Delta E \approx 2$ eV, which is good agreement with the experimental average.[32] (Because of configuration mixing, the experimental average includes both the Q and B bands of porphyrins; see the discussion in ref 32.) The slightly larger splittings in the ab initio molecular orbital energies are consistent with the fact that typical semiempirical values for Coulomb integrals are smaller than the corresponding "theoretical" values.

We next consider the extended Hückel results. In this model, electron repulsion effects are not explicitly included in the Hamiltonian, and the total energy is approximated as a sum of one-electron energies. Hence the one-electron energy differences more closely approximate state energy differences. Indeed, Zerner, Gouterman, and Kobayashi[32] chose their parameters such that

$$\Delta E \equiv \omega_{\pi^*} - \omega_{\pi} \qquad (7)$$

where we have used the symbol "ω" for the eigenvalues of the Hückel Hamiltonian to emphasize the fact that they bear little relation to Hartree-Fock eigenvalues. Since the large Coulomb term of eq 6 is effectively incorporated into the ω's, the Hückel $\pi \rightarrow \pi^*$ splitting itself is about 2 eV (see Figure 2).

In the Xα method we have yet a third relation between the eigenvalues and the total energy:[31,36]

$$\Delta E = \epsilon_{\pi^*}^{X\alpha} - \epsilon_{\pi}^{X\alpha} + \frac{1}{2}[J_{\pi^*\pi^*} + J_{\pi\pi} - 2J_{\pi\pi^*}] + \frac{1}{2}[K_{\pi\pi}{}^0 + K_{\pi^*\pi^*}{}^0 - 2K_{\pi\pi^*}{}^0] \qquad (8)$$

where the exchange term $k_{ij}{}^0$ is

$$K_{ij}{}^0 \equiv -\left(\frac{3}{4\pi}\right)^{1/3} \alpha \int \rho_i \rho_j \rho^{-2/3}\, d\tau \qquad (9)$$

Here ρ_i and ρ_j are the charge densities of orbitals i and j, ρ is the total charge density, and α measures the strength of the effective exchange force (see Table II). For delocalized π orbitals, the Coulomb and exchange sums are small; e.g., since the charge is distributed approximately uniformly around the ring, the Coulomb term in eq 8 is nearly zero with $J_{\pi\pi} \approx J_{\pi^*\pi^*} \approx J_{\pi\pi^*}$. Hence the state energy difference is equal to the orbital energy difference. Thus, as in the Hückel theory, we have a one-electron energy difference of about 2 eV. For other types

Table III. Composition of the SCF Molecular Orbitals[a] for Heme O_2

sym-metry	energy	description	sym-metry	energy	description
		a′ Symmetry			
1a′	−52.60	50.0% $O(2s)_1$ + 33.2% $O(2s)_2$ + 13.0% $O_2 3\sigma_g$	26a′	8.02	71.7% $4p_y$ + 11.3% $O_2 3\sigma_u$ + 9.7% Nσ + 4.7% z^2
2a′	−30.56	37.6% $O(2s)_2$ + 27.6% $O(2s)_1$ + 14.3% $O(2p_y)_1$ + 5.5% $4p_z$ + 4.6% 4s	27a′	10.35	44.6% $O_2 3\sigma_u$ + 27.9% $4p_z$ + 12.7% $4p_y$ + 5.9% z^2
3a′	−20.10	86.4% $O_2 1\pi_u$ + 5.1% z^2	28a′	14.78	35.9% $4p_z$ + 18.8% $O(2s)_1$ + 11.4% $O_2 3\sigma_u$ + 5.1% $O(2s)_2$
4a′	−18.54	70.1% $O_2 3\sigma_g$ + 17.1% $O(2s)_1$			
5a′	−16.51	34.9% Nσ + 33.3% Imσ + 15.3% z^2			a″ Symmetry
6a′	−16.09	38.7% Imσ + 36.4% Nσ + 15.5% 4s	1a″	−18.68	93.5% $O_2 1\pi_u$
7a′	−13.33	90.2% a_{2u}	2a″	−16.63	72.0% Nσ + 28.0% xy
8a′	−13.20	50.7% Nσ + 35.6% e_g + 6.5% $4p_y$	3a″	−14.62	95.9% Imπ
9a′	−13.18	61.9% e_g + 29.9% Nσ + 4.1% yz	4a″	−13.22	54.5% Nσ + 26.7% e_g + 7.1% $4p_x$
*10a′	−11.27	b_{1u}	5a″	−13.09	66.1% e_g + 26.8% Nσ
*11a′	−10.95	60.8% $O_2 1\pi_g$ + 17.5% yz + 16.9% por(π)	6a″	−12.17	b_{2u}
			7a″	−11.76	85.5% Imπ + 4.3% xz
*12a′	−9.95	72.3% e_g + 18.6% $O_2 1\pi_g$ + 4.96% yz	*8a″	−10.60	92.6% Imπ
			*9a″	−9.90	89.2% e_g + 4.2% xz
*13a′	−9.67	80.7% e_g + 9.0% yz	*10a″	−9.57	78.6% e_g + 11.1% xz
*14a′	−9.25	$x^2 - y^2$	*11a″	−8.87	b_{2u}
*15a′	−9.15	98.5% a_{2u}	*12a″	−7.40	a_{1u}
*16a′	−7.03	51.0% e_g + 44.7% yz	*13a″	−6.95	38.2% e_g + 36.6% xz + 19.6% $O_2 1\pi_g$
*17a′	−6.46	98.2% a_{2u}			
*18a′	−0.50	89.5% e_g + 10.1% yz	*14a″	−0.84	79.2% e_g + 19.5% $O_2 1\pi_g$
*19a′	0.96	b_{1u}	*15a″	0.12	63.0% Imπ + 23.3% $O_2 1\pi_g$ + 4.4% xz
20a′	3.50	98.0% e_g			
21a′	4.41	a_{2u}	*16a″	1.06	61.1% Imπ + 19.9% $O_2 1\pi_g$ + 10.8% xz
22a′	4.72	99.6% (e_g and b_{1u})			
23a′	4.76	99.8% (e_g and b_{1u})	*17a″	2.07	71.3% Imπ + 10.2% $O_2 1\pi_g$ + 10.0% xz
24a′	5.73	54.2% z^2 + 20.5% Nσ + 10.9% 4s + 4.2% Imσ			
			*18a″	2.40	b_{2u}
25a′	6.46	52.4% 4s + 14.5% $4p_z$ + 11.5% Imσ + 7.6% z^2	19a″	3.57	92.2% e_g + 4.9% xz
			20a″	3.85	a_{1u}
			21a″	4.77	98.4% e_g
			22a″	6.43	72.0% xy + 28.0% Nσ
			23a″	8.68	83.9% $4p_x$ + 9.9% Nσ

[a] Notation: Nσ, σ orbitals of the four pyrrole nitrogens on the heme; Imσ, σ orbital of the axial nitrogen; Imπ, π orbitals of the imidazole. Energies are in electron volts (eV). Iron and oxygen 2s contributions greater than 4% are listed; other contributions greater than 10% are listed. Orbitals denoted with an asterisk are included in the double CI calculation.

of transitions, such as charge-transfer states, the cancellation in eq 8 will not be complete, and the one-electron energy difference will no longer approximate the true state separation.

Having sketched the reasons for the gross differences seen in Figure 2, we can analyze in detail the nature of the molecular orbitals and their energies. The labels in the diagram give the dominant characteristic of each orbital; more complete information for the PPP calculation is contained in Tables III and IV. We can consider the orbitals as arising primarily from the four components of the complex: (1) porphyrin, (2) iron, (3) dioxygen, and (4) imidazole.

(1) Porphyrin. As might be expected, the porphyrin π orbitals are not much affected by the iron or the axial ligands, and for the most part they appear to be nearly unchanged from their positions in the free porphyrin. The highest occupied π orbitals are the pair a_{1u}, a_{2u}; these correspond to the $m_l = \pm 4$ states of a free electron model of porphyrin,[37] in which 18 π electrons are considered to move in a ring of uniform potential. The lowest unoccupied π^* orbital has e_g symmetry in D_{4h} and corresponds to $m_l = \pm 5$. The major perturbation of the porphyrin π orbitals involves the occupied e_g orbitals, which have the proper symmetry to mix with the iron $3d_{xz}$ and $3d_{yz}$ orbitals. This mixing is rather strong in all but the ab initio calculation; the result is that mixed orbitals appear at two energies, one slightly below the top occupied π orbitals of the porphyrin, and the other somewhat lower. (These have been labeled "xz/e_g" and "yz/e_g" in Figure 2; they correspond to 13a′, 16a′ and 10a″, 13a″ in Table III.) In the ab initio calculation only the lower level has significant iron 3dπ character; we shall see the consequences of this below.

(2) Iron. The remaining iron 3d orbitals (d_{z^2}, d_{xy}, and $d_{x^2-y^2}$) do not interact as strongly with the rest of the molecule as do the dπ orbitals. The occupied $d_{x^2-y^2}$ orbital is just below the top four porphyrin π orbitals (labeled a_{1u}, a_{2u}, b_{2u}, and a_{2u}) except in the Hückel calculation, where it is higher in energy, between the highest occupied π orbitals (a_{1u}, a_{2u}). We noted in an earlier study on copper porphyrin[26] that the Hückel method places the d orbitals at higher energy than does the Xα method. In that example, the experimental oxidation–reduction behavior appeared to support the Xα ordering of levels. The situation is less clear in iron porphyrins, but the results we obtain below for charge-transfer transitions suggest that the Xα energy scheme is valid.

(3) Dioxygen. In all four treatments there is an important low-energy empty orbital comprised primarily of the $3d_{xz}$ orbital on iron and the out-of-plane π_g^* molecular orbital of O_2. This orbital is antibonding between Fe and O^1, and between O^1 and O^2. It is related to the lowest unoccupied ($2b_1$) orbital of ozone[38] and forms part of the basis for the analogy between ozone and FeO_2. This orbital is labeled "$xz/O_2\pi^*$" in Figure 2. It is the lowest unoccupied orbital in the Hückel and Xα calculations, and is third lowest in the PPP and Hartree–Fock results. In the PPP calculation the iron character is replaced by charge density on the imidazole. We shall see below that single excitations into this orbital are involved in several of the

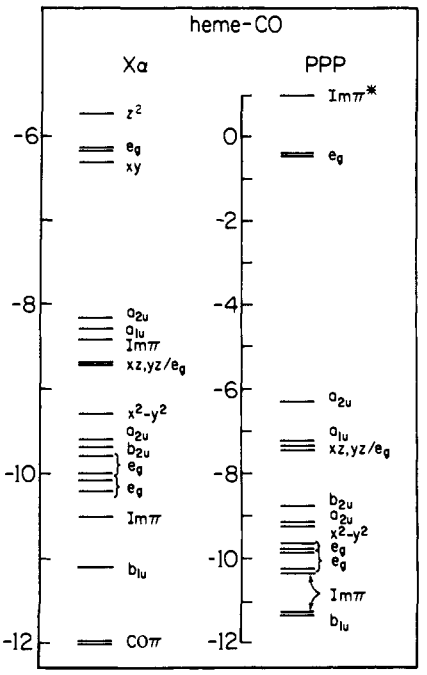

Figure 3. Molecular orbital energies for heme-CO.

low-lying excited states of heme-O_2, and that double excitations into this orbital are important in describing correlation effects and in producing a singlet ground state. The existence of such an orbital in all four calculations makes it likely that this is a genuine feature of the MO model and not an artifact of a particular set of approximations.

The analogous orbital formed from the in-plane component of O_2 π_g* and iron $3d_{yz}$ is occupied in the molecular orbital description. Its energy is near the top of the valence band in the Hückel and Xα descriptions, but is 5–6 eV below the highest occupied molecular orbital in the PPP and Hartree–Fock calculations. This splitting between the in-plane and out-of-plane components of the O_2 π_g* orbital is due to the asymmetric binding geometry and is central to the Pauling explanation of the diamagnetism of oxyhemoglobin. It is significant that this feature appears in all four calculations. In the perpendicular geometry proposed by Griffith, or in asymmetric geometries close to it, this splitting is in the opposite direction, with an occupied out-of-plane orbital and an unoccupied in-plane orbital.[33,39] We restrict the discussion in this paper to the Pauling geometry.

(4) Imidazole. In the Xα and extended Hückel calculations, the imidazole π orbitals do not interact strongly with the rest of the molecule. This result is in line with Hartree–Fock studies on iron and cobalt–imidazole complexes,[35,39] which view the imidazole as neither a π donor nor a π acceptor; that is, the imidazole has little effect on the electronic structure of the rest of the complex. In the PPP calculations, there is extensive mixing of the unoccupied imidazole π orbitals with iron $3d_{xz}$ and the oxygen p_x orbitals. As a result, there are three low-lying virtual orbitals with such character, 15a″, 16a″, and 17a″ (see Table III). This appears to be a consequence of an accidental near degeneracy of imidazole and oxygen orbitals which is absent in the other calculations; the population analysis given below supports the view that there is little redistribution of the imidazole charge. This mixing does lead to complications in the interpretation of the CI results to be discussed in section IV. Since the mixing may be sensitive to the geometry and parameters we have assumed, it is not clear how important it is in real compounds; e.g., the effect of the asymmetric imidazole position[14,42] is not known.

Table IV. Composition of the SCF Molecular Orbitals[a] for Heme CO

sym-metry	energy	description
		a′ Symmetry
1a′	−49.10	56.6% O(2s) + 29.0% C(2s) + 13.5% CO(5σ)
2a′	−21.76	37.2% C(2s) + 23.7% O(2s) + 22.2% CO(6σ) + 7.9% 4s + 4.8% $4p_z$
3a′	−17.98	97.7% CO($1\pi_y$)
4a′	−17.91	75.7% CO(5σ) + 6.1% O(2s) + 5.1% Imσ + 5.5% z^2
5a′	−16.11	68.8% Nσ + 15.7% z^2 + 11.5% 4s
6a′	−15.06	71.7% Imσ + 9.2% $4p_z$
7a′	−13.21	96.2% a_{2u}
8a′	−13.07	93.1% e_g + 5.7% yz
9a′	−13.04	85.9% e_u + 12.3% $4p_y$
10a′	−11.20	b_{1u}
*11a′	−10.20	60.8% e_g + 37.0% yz
*12a′	−9.71	95.8% e_g + 3.4% yz
*13a′	−9.18	$x^2 - y^2$
*14a′	−9.10	a_{2u}
*15a′	−7.33	57.6% e_g + 38.7% yz
*16a′	−6.34	a_{2u}
*17a′	−0.53	91.4% e_g + 5.56% yz
*18a′	1.01	b_{1u}
*19a′	2.59	82.3% CO($2\pi_y$) + 4.8% $4p_y$ + 4.4% yz
20a′	3.59	93.4% eg
21a′	4.41	84.3% a_{2u} + 5.7% z^2 + 5.6% $4p_z$
22a′	4.78	e_g + b_{1u}
23a′	4.82	e_g + b_{1u}
24a′	5.16	62.6% z^2 + 11.5% Nσ + 10.6% a_{2u} + 7.3% Imσ
25a′	6.54	61.6% 4s + 15.5% Nσ + 10.6% $4p_z$
26a′	8.03	81.8% $4p_y$ + 11.1% Nσ
27a′	9.52	52.3% $4p_z$ + 24.3% C($2P_z$) + 6.2% 4s + 5.3% z^2
28a′	13.16	80.8% CO(6σ) + 12.9% $4p_z$
		a″ Symmetry
1a″	−17.98	97.7% CO($1\pi_x$)
2a″	−16.53	70.7% Nσ + 29.3% xy
3a″	−14.15	96.4% Imπ
4a″	−13.09	71.1% e_g + 17.1% e_u + 5.0% xz
5a″	−13.05	66.3% e_u + 20.8% e_g + 9.6% $4p_x$
6a″	−12.07	b_{2u}
7a″	−11.27	82.3% Imπ + 8.5% xz
*8a″	−10.29	65.0% Imπ + 20.3% e_g + 13.9% xz
*9a″	−9.87	55.9% e_g + 36.7% Imπ + 6.8% xz
*10a″	−9.66	79.5% e_g + 8.2% xz + 11.7% Imπ
*11a″	−8.78	b_{2u}
*12a″	−7.31	a_{1u}
*13a″	−7.24	55.0% e_g + 38.0% xz
*14a″	−0.54	91.5% e_g + 5.4% xz
*15a″	0.95	96.3% Imπ
*16a″	2.09	79.2% Imπ + 17.3% CO($2\pi_x$)
*17a″	2.56	b_{2u}
*18a″	2.76	61.7% CO($2\pi_x$) + 19.7% Imπ + 4.7% xz
19a″	3.62	8.95% e_g + 3.5% xz
20a″	3.87	a_{1u}
21a″	4.81	e_g
22a″	6.29	70.7% xy + 29.3% Nσ
23a″	8.12	81.4% $4p_x$ + 10.9% Nσ

[a] See footnote to Table III.

Orbital energies for heme-CO are shown in Figure 3. The principal change from the O_2 complex is in the π* orbital of CO. Here both the in-plane and out-of-plane components are unoccupied and lie very high in energy since the carbon atomic orbitals are higher in energy than those of oxygen. This means

Table V. PPP Electronic Populations

(1) Porphine Nitrogen Orbitals

	π	σ
Fe porphine ($S = 0$)	1.35	1.65
heme–O_2	1.33	1.60
heme–CO	1.30	1.58

(2) Imidazole Orbitals

	N1π	C2π	N3σ	N3π	C4π	C5π	total π
imidazole[a]	1.70	1.12	2.00	1.01	1.12	1.05	6.00
heme–O_2	1.65	1.02	1.65	1.23	1.12	1.00	6.03
heme–CO	1.66	1.03	1.68	1.19	1.12	1.01	6.02

(3) Dioxygen Orbitals[b]

	center oxygen					terminal oxygen				
	2s	$2p_x$	$2p_y$	$2p_z$	total	2s	$2p_x$	$2p_y$	$2p_z$	total
$O_2(^1\Delta_g)$[a]	1.90	1.04	1.96	1.10	6.00	1.90	1.04	1.96	1.10	6.00
heme–O_2	1.59	1.27	1.88	1.12	5.86	1.81	1.14	1.99	1.14	6.08
O_3	1.80	1.21	1.43	1.22	5.65	1.93	1.40	1.98	0.87	6.18

(4) Carbon Monoxide Orbitals

	carbon					oxygen				
	2s	$2p_x$	$2p_y$	$2p_z$	total	2s	$2p_x$	$2p_y$	$2p_z$	total
CO[a]	1.74	0.63	0.63	1.08	4.09	1.74	1.37	1.37	1.44	5.91
heme–CO	1.45	0.70	0.70	0.43	3.79	1.73	1.40	1.40	1.44	5.97

[a] Free ligand. [b] z axis passes through the O–O bond.

that the important correlation and excitation effects associated with the π^* orbital in the O_2 adduct will be nearly absent here. Also, the strong mixing involving the imidazole π^* orbitals is not present (see Table IV, which gives the composition of the heme–CO orbitals).

Although orbital descriptions such as these are useful in providing a qualitative understanding of the electronic structure, they miss many features of the charge reorganization that takes place. Some of these can be measured by effective charges and bond orders, which we present below.

B. Population Analysis. In the PPP approximation, the molecular orbitals, Ψ_i, are expressed as a linear combination of atomic orbitals ϕ_μ:

$$\Psi_i = \sum_\mu C_{i\mu}\phi_\mu \tag{10}$$

For a closed-shell system, the density matrix $P_{\mu\nu}$ is defined as

$$P_{\mu\nu} = 2\sum_i^{\text{occ}} C_{i\mu}C_{i\nu} \tag{11}$$

where the summation is over the occupied molecular orbitals. **P** transforms under coordinate rotations like the overlap integral matrix **S**. The diagonal element $P_{\mu\mu}$ represents the charge density in atomic orbital ϕ_μ; the off-diagonal element $P_{\mu\nu}$ represents the bond order between orbitals ϕ_μ and ϕ_ν. The quantity

$$Q_A = \sum_{\mu\in A} P_{\mu\mu} \tag{12}$$

is invariant under rotation and represents the total charge of atom A. (In eq 12 the sum is over the atomic orbitals of atom A.) However, the total bond order between two atoms A and B cannot be generalized to

$$P_{AB} = \sum_{\substack{\mu\in A \\ \nu\in B}} P_{\mu\nu} \tag{13}$$

because the quantity P_{AB} so defined is not invariant under rotational transformations. For this reason, bond orders reported below are always given between atomic orbitals represented in a coordinate system that has its z axis passing through the two atomic sites of interest. Thus, these numbers correspond to those conventionally used to rationalize the bond strengths of diatomic molecules.

The PPP charge densities are given in Table V, where comparison is made with calculations on various fragments: imidazole, oxygen, and iron porphyrin. The iron atom in heme–O_2 has a net charge of +0.45 and a total 3d population of 6.19, which is consistent with a ferrous ion assignment. Although the formal oxidation state is +2, electron donation from the five nitrogen ligands partially neutralize the metal. Pauling[7] originally argued that the porphyrin alone could neutralize the iron, but the present results suggest that σ donation from the imidazole is also necessary. The π system of imidazole appears to be only slightly perturbed by complexation with iron; this is in accord with the ab initio and Hückel results.[35,39] Complexation of Fe^{2+} to the porphyrin dianion involves σ donation of 0.4 electron per nitrogen and π back-donation of 0.1 electron per nitrogen. An additional 0.35 electron is donated to iron from the imidazole σ system. Since the ferrous ion is nearly neutralized by its five nitrogen ligands, the binding of the oxygen molecule is mainly covalent, with little charge transfer.

Details of the change in oxygen populations relative to the free molecule are also given in Table V. These show that the σ donation to the iron (primarily from the 2s orbital of O^1) is almost exactly balanced by π back-donation (into the $2p_x$ orbitals of both O^1 and O^2). The back-donation is into an antibonding orbital and it appears that this is primarily responsible for the weakening of the O–O bond.[2] Table V also shows how the populations in heme–O_2 compare with those in ozone. The most significant difference is in the $2p_y$ population of O^1; this is larger in hemoglobin because the in-plane Fe–O^1 π bond is more strongly polarized toward O^1 than is the corresponding bond in ozone. Aside from this difference, the populations in heme–O_2 and ozone are surprisingly close.

Table VI. Iron Atom Orbital Populations

	4s	$4p_x$	$4p_y$	$4p_z$	$3d_{x^2-y^2}$	$3d_{xz}$	$3d_{yz}$	$3d_{z^2}$	$3d_{xy}$	net
					Heme–O_2					
EHT[a]	0.29	0.14	0.12	0.16	2.00	1.25	1.96	0.84	0.99	+0.25
Xα	0.73	0.48	0.47	0.62	1.98	1.66	2.00	1.09	0.81	−1.83
PPP SCF	0.52	0.26	0.25	0.33	2.00	1.36	1.74	0.53	0.56	+0.45
PPP CI[b]	0.52	0.26	0.25	0.33	2.00	1.28	1.69	0.53	0.56	+0.57
HF[c]	0.15	0.11	0.11	0.07	1.91	1.90	1.96	0.22	0.33	+1.22
					Heme–CO					
EHT[a]	0.26	0.10	0.09	0.20	2.00	1.71	1.72	0.88	0.86	+0.18
Xα	0.74	0.46	0.45	0.62	1.95	1.95	1.98	0.98	0.76	−1.88
PPP	0.54	0.26	0.26	0.34	2.00	1.70	1.73	0.51	0.59	+0.08

[a] Reference 5. [b] Results from CI calculation; see section IIIE. [c] Reference 33.

Table VII. Self-Consistent Xα Potentials[a]

(1) Iron

			heme–O_2		heme–CO		heme–CN	
r^b	Fe ($3d^64s^2$)	Fe^+ ($3d^54s^2$)	$V(r)$	q^c	$V(r)$	q^c	$V(r)$	q^c
0.0254	−932.055	−932.623	−932.102	0.083	−932.081	0.046	−932.223	0.296
0.0687	−297.877	−298.453	−297.922	0.078	−297.900	0.040	−298.042	0.286
0.1434	−115.492	−116.083	−115.540	0.080	−115.518	0.044	−115.658	0.281
0.2689	−45.953	−46.559	−46.002	0.081	−45.979	0.043	−46.117	0.271
0.4722	−17.676	−18.277	−17.724	0.081	−17.701	0.042	−17.840	0.273
0.8547	−5.181	−5.743	−5.237	0.100	−5.213	0.057	−5.358	0.315
1.1655	−2.511	−3.018	−2.591	0.157	−2.568	0.112	−2.720	0.412
1.5480	−1.276	−1.714	−1.409	0.303	−1.390	0.260	−1.549	0.623
1.9783	−0.727	−1.098	−0.954	0.612	−0.939	0.571	−1.100	1.005
2.3609	−0.480	−0.821	−0.854	1.098	−0.839	1.053	−0.994	1.507
2.7434	−0.344	−0.649	−0.900	1.822	−0.878	1.751	−1.019	2.213

(2) Oxygen

		heme–O_2		O_3		heme–CO	
r^d	O ($2s^22p^4$)	central	terminal	central	terminal	terminal	NaO_2
0.0376	−197.149	−197.198	−197.150	−197.305	−197.104	−197.119	−197.022
0.1018	−63.881	−63.933	−63.889	−64.032	−63.833	−63.853	−63.750
0.2125	−25.084	−25.144	−25.102	−25.226	−25.034	−25.062	−24.957
0.3984	−10.020	−10.110	−10.063	−10.154	−9.984	−10.030	−9.938
0.6994	−3.842	−3.982	−3.924	−3.970	−3.835	−3.908	−3.840
1.2660	−1.101	−1.390	−1.286	−1.293	−1.199	−1.335	−1.295
1.4431	−0.815	−1.195	−1.077	−1.097	−0.999	−1.149	−1.074
1.5848	−0.655	−1.125	−1.000	−1.029	−0.928	−1.083	−0.907

[a] Energies in hartree atomic units. [b] Distance from iron nucleus in atomic units. [c] Estimated from eq 14. [d] Distance from oxygen nucleus in atomic units.

Table VI gives details of the iron atom population in each of the calculations; included also is a PPP CI calculation discussed further in section IIIE. There are large differences in the results for the orbitals that are formally not occupied, i.e., $3d_{z^2}$, $3d_{xy}$, 4s, and 4p. The Xα calculation places the most charge in these orbitals, and results in an iron with a net negative charge. We shall show below that this is a consequence of the overlapping sphere approximation, and is not a good measure of the true environment in the vicinity of the iron atom. The Hückel and PPP calculations put about the same total charge in these orbitals, while there is substantially less in the ab initio Hartree–Fock results. Hence the latter does not lead to the neutralization of the iron atom by σ donation from the nitrogens. It is difficult to say whether this is a correct description or is the result of the limited basis set or the Mulliken charge analysis; a double ζ calculation[35] on a simplified model for the FeO_2 system yields an increase (by 0.5 e) in the net positive charge of the iron. We discuss the details of the 3d-orbital populations below in connection with the Mössbauer spectrum.

The charge distribution of heme–CO is also given in Tables V and VI. Little charge reorganization is observed upon incorporation of CO ($S = 0$) into iron porphin ($S = 0$). The amount of σ forward donation from the CO ligand is 0.45 electron, comparable to that in O_2, while the π back-donation is only 0.20 electron, less than that for the O_2 ligand. The difference is the result of the high energy of the CO π* orbitals, which makes them less attractive as π acceptors. Hence in the CO complex the iron is more negative than in the O_2 complex, and the carbon atom is positive (+0.21).

The Mulliken population parameter defined in eq 12 is a natural one in the ZDO approximation. It is not simple to find equivalent measures for Xα wave functions. A parameter commonly reported is the amount of charge inside each cell; as we have shown before,[26] this is strongly dependent upon the sphere radii and does not correlate well with the usual chemical indexes of charge distribution. It is more instructive to consider the self-consistent potential, which includes Coulombic and effective exchange contributions. In Table VII we list the iron and oxygen potentials as a function of the distances from the respective nuclei; included for reference are various atomic configurations, results from the low-spin ferric compound heme–CN, and the Xα potentials for O_3 and NaO_2. These potentials reflect the average environment seen by electrons

at various points in space, and offer a quantitative measure of the local changes accompanying the formation of chemical bonds. We draw three principal conclusions from the data in Table VII: (1) There is no evidence of the formation of a superoxide anion. The potential for O^1 in heme-O_2 is more negative than that for atomic oxygen, indicating that the atom has a small net positive charge in the molecular environment. The potentials for heme-O_2 do not compare at all well with those for NaO_2. This is in agreement with the PPP results discussed above. (2) The iron in heme-O_2 carries a slight positive charge compared to an isolated iron atom ($3d^64s^2$), but the difference is small. It is definitely not as large as the charge on iron in heme-CN. We can approximate the effective charge by linear interpolation between atomic states of the configurations $3d^64s^2$ and $3d^54s^2$:

$$q^{\text{mol}} = \frac{V(r;\text{mol}) - V(r;\text{Fe}^0)}{V(r;\text{Fe}^{+1}) - V(r;\text{Fe}^0)} \qquad (14)$$

For values of r less than half the distance to the nearest neighbor, the value of q^{mol} is nearly constant, and may be taken as characteristic of the atomic charge. (As one goes to larger r, the molecular potential begins to see the incompletely shielded nuclear potential from the next atom; this makes the potential more negative, and in this region the simple interpolation of eq 14 is not appropriate.) In this approximation, the iron in heme-O_2 has a net charge of +0.08, while that in heme-CN has a charge of +0.28. (3) The iron in heme-CO has a potential that is nearly identical with that of an isolated atom with configuration $3d^64s^2$. The net charge from eq 14 is +0.04. This supports the argument that heme-CO approaches an idealized ferrous low-spin complex.

Earlier[2] we interpreted our results as describing heme-O_2 to be intermediate between the first two reference states described in the Introduction. This conclusion may be compared to the results of a semiempirical valence bond (VB) calculation by Seno et al.[41] Their results indicate that the ground state of the FeO_2 unit consists of almost equal weight triplet-triplet coupled and singlet-singlet coupled states. The electronic configuration for the covalent singlet-singlet coupled state is

$$\text{Fe}[(d_{x^2-y^2})^2(d_{yz})^2(d_{xz})^2(d_{z^2})^0(d_{xy})^0] - \text{O}^1[(2p_{x'})^{1.5}(2p_{y'})^{1.5}(2p_{z'})^1] - \text{O}^2[(2p_{x'})^{1.5}(2p_{y'})^{1.5}(2p_{z'})^1]$$

and for the covalent triplet-triplet coupled state is

$$\text{Fe}[(d_{x^2-y^2})^2(d_{yz})^2(d_{xz})^1(d_{z^2})^1(d_{xy})^0] - \text{O}^1[(2p_{x'})^1(2p_{y'})^2(2p_{z'})^1] - \text{O}^2[(2p_{x'})^1(2p_{y'})^2(2p_{z'})^1]$$

where O^1 represents the center oxygen and O^2 represents the terminal oxygen. The $x'y'z'$ axes correspond to a local coordinate system oriented with respect to the oxygen molecule; the z' axis is along the O-O bond and the x' axis is perpendicular to the Fe-O-O plane. An equal-weight average of these two states gives a configuration of

$$\text{Fe}[(d_{x^2-y^2})^2(d_{yz})^2(d_{xz})^{1.5}(d_{z^2})^{0.5}(d_{xy})^0] - \text{O}^1[(2p_{x'})^{1.25}(2p_{y'})^{1.75}(2p_{z'})^1] - \text{O}^2[(2p_{x'})^{1.25}(2p_{y'})^{1.75}(2p_{z'})^1]$$

From Table V, the present PPP calculations indicate that the electronic configuration of the FeO_2 unit in hemoglobin is given by

$$\text{Fe}[(d_{x^2-y^2})^{2.0}(d_{yz})^{1.74}(d_{xz})^{1.36}(d_{z^2})^{0.53}(d_{xy})^{0.56}] - \text{O}^1[(2p_{x'})^{1.27}(2p_{y'})^{1.88}(2p_{z'})^{1.12}] - \text{O}^2[(2p_{x'})^{1.14}(2p_{y'})^{1.99}(2p_{z'})^{1.14}]$$

which is very near the equal-weight average of the VB results. The minor differences in electronic population between the two stem mainly from the fact that, in the VB calculation, only three atoms (Fe-O-O) are considered and orbitals of an isolated oxygen molecule were used as basis functions. Therefore, no $3d_{xy}$ population is obtained in the VB calculation, and the two oxygen atoms in the FeO_2 unit retain the symmetry of the isolated ligand.

Table VIII. Bond Orders

(1) Ozone: z Axis Passes through the O-O Bond

terminal O	center O p_x	center O p_y	center O p_z
p_x	0.6917	0.0	0.0
p_y	0.0	0.1003	−0.0220
p_z	0.0	−0.0953	−0.8577

(2) HbO_2: z Axis Passes through the O-O Bond

	center O p_x	center O p_y	center O p_z
p_x	0.7710	0.0	0.0
p_y	0.0	0.0331	0.0345
p_z	0.0	−0.0180	−0.7929

(3) HbO_2: z Axis Passes through the O-Fe-N Bonds

Fe	center O p_x	center O p_y	center O p_z
4s	0.0	−0.0282	0.2256
$4p_x$	0.1890	0.0	0.0
$4p_y$	0.0	0.2224	0.0770
$4p_z$	0.0	0.0749	−0.2659
xz	−0.5006	0.0	0.0
yz	0.0	−0.0838	0.0280
z^2	0.0	0.0672	0.3726
x^2-y^2	0.0	0.0	0.0
xy	0.0009	0.0	0.0

(4) CO Free Ligand

C	O $2p_x$	O $2p_y$	O $2p_z$
$2p_x$	0.9306	0.0	0.0
$2p_y$	0.0	0.9306	0.0
$2p_z$	0.0	0.0	−0.7169

(5) HbCO: z Axis Passes through the C-O Bond

C	O $2p_x$	O $2p_y$	O $2p_z$
$2p_x$	0.8805	0.0	0.0
$2p_y$	0.0	0.879⁻	0.0
$2p_z$	0.0	0.0	−0.6914

(6) HbCO: z Axis Passes through the Fe-C-O Bond

Fe	C $2p_x$	C $2p_y$	C $2p_z$
4s	0.0	0.0	0.2318
$4p_x$	0.0834	0.0	0.0
$4p_y$	0.0	0.0825	0.0
$4p_z$	0.0	0.0	−0.2672
z^2	0.0	0.0	0.2939
xz	−0.3334	0.0	0.0
yz	0.0	−0.3379	0.0
x^2-y^2	0.0	0.0	0.0
xy	0.0	0.0	0.0

C. Bond Orders. Table VIII gives the PPP bond orders from eq 11. Parts (1) and (2) show the close resemblance between the O-O bonds in ozone and in heme-O_2. This analogy is supported by the observed stretching frequencies, which suggest that the force constants should be nearly identical for the two molecules.[2,4] From the point of view of the present calculations, the fact that the O_2^- force constant is also in the same range appears to be a coincidence.

Part (3) of Table VIII gives bond orders for the Fe-O^1 bond. An analogy with ozone can still be discussed, although the interpretation is less clear since the orbital overlaps are not the same. The density matrix element connecting Fe $3d_{xz}$ with O^1 $2p_x$ (0.50) is smaller than the analogous value in O_3 ($2p_x - 2p_x = 0.69$), but the Fe-O^1 π bond is additionally strengthened by a bonding interaction with Fe $4p_x$ (Fe $4p_x - O^1$ $2p_x = 0.19$). Similar comments apply to the in-plane bonds, where the $3d_{yz} - 2p_y$ and $3d_{z2} - 2p_z$ overlap populations are smaller than their counterparts in ozone.

Bond orders for the C-O bond in the free ligand and in heme-CO are listed in part (4) of Table VIII. There is a reduction of about 0.13 in the total CO bond order upon incorporation into iron porphyrin (2.58 to 2.45). This may be compared to the reduction of 0.19 upon going from O_2 $^1\Delta_g$ (1.79) to HbO_2 (1.60). In each case this can qualitatively explain the reduction in stretching frequencies: ν_{O_2} goes from 1484 cm^{-1} in the free ligand ($^1\Delta_g$) to 1160 cm^{-1} in model heme compounds[4] and to ~1100 cm^{-1} in hemoglobin and myoglobin;[42] ν_{CO} is changed from 2143 cm^{-1} in the gas to 1970 cm^{-1} in model compounds[4] and ~1950 cm^{-1} in the protein.[43] In neither case is the lowering of the stretching frequency indicative of charge transfer.

The bond orders in the porphyrin skeleton may be checked by applying standard relations between bond lengths and π-bond orders:[21]

$$r_{\mu\nu}(\text{C-N}) = 1.458 - 0.18P_{\mu\nu}$$

$$r_{\mu\nu}(\text{C-C}) = 1.517 - 0.18P_{\mu\nu}$$

On the left-hand side of Figure 1 we present the bond distances estimated from these formulas. They are all within 0.02 Å of the assumed values given on the right-hand side. This indicates that the porphyrin π structure is a reasonable one.

D. Mössbauer Quadrupole Splitting. One of the more striking differences between O_2 and CO hemoglobin is in the quadrupole splitting seen in the Mössbauer spectrum. At 1.2 K, the quadrupole splitting, ΔE_Q, for oxyhemoglobin is 2.24 mm/s; this is found to be temperature dependent, falling to about 1.9 mm/s at 195 K.[3,44] Analysis of the spectrum in a magnetic field shows that the principal component of the electric field gradient is negative and in the heme plane.[44] Nearly identical spectra are seen in oxymyoglobin[45] and in several model compounds,[46,47] indicating that the electric field gradient at the iron is insensitive to the protein. Of particular interest is the fact that while the model compound is disordered due to different O_2 and imidazole orientations (see above), the MbO_2 crystal is not.[14] For carboxyhemoglobin the quadrupole splitting is much smaller (0.35 mm/s[43,44]) and is temperature independent, with a positive principal field gradient nearly perpendicular to the heme plane. Hence there are significant differences in the iron environment even though both complexes are formally low-spin ferrous.

Procedures for calculating Mössbauer quadrupole splittings have been described previously.[44,48] In zero magnetic field two peaks are seen in the spectrum, separated by

$$\Delta E_Q = \frac{1}{2} eQV_{zz}\left(1 + \frac{\eta^2}{3}\right)^{1/2} \tag{15}$$

where the asymmetry parameter η is

$$\eta \equiv \frac{V_{xx} - V_{yy}}{V_{zz}} \tag{16}$$

The symbol Q represents the quadrupole moment of the iron nucleus, which we take to be 0.20 b, e is the electron charge, and the V_{kk} are the principal components of the electric field gradient (EFG) at the iron nucleus. We assume that the field gradient arises from two contributions, a "valence" term from orbitals centered on the iron

Table IX. Xα Radial Expectation Values

orbital	energy, eV	% 3d	$\langle r^{-3}\rangle$, au
	Atom		
Fe ($3d^64s^2$)	−7.42	100	5.03
Fe^+ ($3d^54s^2$)	−21.61	100	5.62
	Molecule		
xz/e_g	−10.86	24	4.06
yz/e_g	−10.43	30	4.34
$x^2 - y^2$	−9.75	95	4.85
yz/e_g	−9.17	31	5.14
xz/e_g	−9.16	34	5.14
$yz/O_2\pi^*$	−8.52	26	5.49
$xz/O_2\pi^*$	−7.62[a]	19	5.86
xy	−6.82[a]	75	6.09
	Averages over All Occupied Molecular Orbitals		
t_{2g}	$x^2 - y^2$		4.72
	xz		4.45
	yz		4.47
e_g	z^2		1.95
	xy		2.09

[a] Unoccupied in the ground state.

$$V_{kl}^{\text{val}} = -e(1 - \gamma_0)\left\langle\frac{3r_kr_l - \delta_{kl}r^2}{r^5}\right\rangle \tag{17}$$

and a "lattice" term arising from the ligands

$$V_{kl}^{\text{lat}} = e(1 - \gamma_\infty)\sum_j q_j\frac{3R_kR_l - \delta_{kl}R^2}{R^5} \tag{18}$$

Here $\mathbf{r}$ is the vector from the iron nucleus to an electron, $\mathbf{R}$ is the vector to a ligand with charge q_j, and $(1 - \gamma_0)$ and $(1 - \gamma_\infty)$ are Sternheimer factors, which we take to be 0.68 and 12, respectively.[44] The expectation value in the valence contribution can be factored into the product of an angular integral, which can be performed analytically, and the radial integral

$$\langle\phi|r^{-3}|\phi'\rangle \equiv \int_0^\infty \phi(r)\frac{1}{r^3}\phi'(r)r^2\,dr \tag{19}$$

where ϕ and ϕ' are iron radial wave functions. In the Xα calculation the integrals can be determined directly from the wave functions,[26,30] while for the PPP calculation empirical values must be used. Since the field gradient is a spherical tensor of rank two, the only radial integrals needed are $\langle 3d|r^{-3}|3d\rangle$, $\langle 4p|r^{-3}|4p\rangle$, and $\langle 3d|r^{-3}|4s\rangle$. Following Trautwein,[44] we shall in the PPP model take the first of these to be 4.90 au and the second to be ⅓ of this value. The value of $\langle 3d|r^{-3}|4s\rangle$ is less than 2×10^{-3} au[49] and may be ignored. Inner shell polarization effects are assumed to be adequately described by the Sternheimer factor.

The quadrupole splitting calculated in this manner from the PPP SCF wave function is −2.34 mm/s. Since we have used ΔE_Q to determine the iron-ligand penetration integral (see Appendix), the agreement with experiment is expected. The Xα results are more significant in this respect because they do not involve any empirical parameters. In particular, the actual $\langle r^{-3}\rangle$ expectation values are used for each orbital, rather than values assumed from atomic calculations. The variation of these values with orbital energy is a significant effect,[26] as shown in Table IX. For example, most of the population of iron d_{z^2} and d_{xy} character is not in antibonding orbitals, but rather in low-lying bonding combinations whose radial distributions are more diffuse than those for 3d orbitals in isolated atoms. On the other hand, electrons in antibonding orbitals are more compressed and have higher values of $\langle r^{-3}\rangle$. The effects of this are illustrated in the second part of Table IX, which gives values averaged over all occupied orbitals. The t_{2g} orbitals have radial expectation values only slightly smaller than that of the

Table X. Mössbauer Parameters[a,b]

	heme–O_2					heme–CO			
method	EHT	Xα	PPP SCF	PPP[c] CI	HF	EHT	Xα	PPP SCF	PPP[c] CI
V_{xx}	0.98	1.15	0.16	0.14	0.0	−0.48	−0.13	−0.62	−0.70
V_{yy}	−3.06	−1.43	−2.02	−2.25	−0.35	−0.52	−0.16	−0.79	−0.79
V_{zz}	2.09	0.29	1.85	2.11	0.35	1.01	0.29	1.41	1.48
ΔE_Q	−3.13	−1.52	−2.24	−2.52	0.40	1.01	0.29	1.41	1.48
η	0.36	0.60	0.84	0.87	1.0	0.04	0.10	0.12	0.06

[a] Estimated from d-orbital populations alone; see text. [b] In ^{57}Fe Mossbauer units of mm/s. [c] Results of CI calculation; see section IIIE.

free atom, while the occupied orbitals of e_g character have values less than half as large. Hence the e_g electrons are not as effective as their t_{2g} counterparts in producing a field gradient at the iron nucleus.

The Xα calculation gives $\Delta E_Q = -1.62$ mm/s and $\eta = 0.15$; the principal component of the field gradient is negative and along the y axis. It is difficult to compare these numbers with experiment because of the observed temperature dependence. Spartalian et al.[47] have interpreted the results in a model compound on the basis of a thermal equilibrium between two conformations differing by a rotation of the oxygen molecule by 90° about the Fe–O bond; this corresponds to the disorder seen in X-ray studies of the model compound,[13] but not in myoglobin.[14] Our results correspond well to those of the postulated low-energy conformer: in ^{57}Fe Mössbauer units of mm/s our values for eQV_{ii} are −3.23, 1.84, and 1.36, with the smallest value normal to the heme plane; values from the fit to experiment[47] are −4.18, 2.57, and 1.60, in the same axis system. We emphasize that this comparison may be misleading because the fit to experiment involves some assumptions that may not hold, and there is some latitude in the final parameters. Nonetheless, we feel that it is significant that the major qualitative conclusions of the experimental analysis are reproduced in the Xα calculation; that is, there is a large quadrupole splitting and the principal component of the field gradient is negative and in the heme plane.

For the present system the quadrupole splitting is dominated by the d orbitals, since the contributions from the 4p orbitals and from the ligands approximately cancel. For example, in the Xα calculations the d orbitals alone yield $\Delta E_Q = -1.52$ mm/s compared to the value of −1.62 for a complete calculation; in the PPP calculation the d orbitals give −2.24 mm/s, while the complete calculation gives −2.34. (It should be noted that such a result may not hold for five-coordinate hemes, where the asymmetry in the ligand distribution is much greater.) We can use this fact to interpret the results of various MO calculations in terms of d-orbital occupations. The populations of Table VI yield the field gradients of Table X. The three semiempirical calculations all yield a negative principal EFG component along the y molecular axis, with the magnitudes in rough agreement with experiment. The ab initio calculation, on the other hand, has a quadrupole splitting much smaller than experiment. This follows from the populations, which are very close to those of the idealized $(t_{2g})^6$ structure which has no net field gradient. The remaining calculations give a marked population difference between the d_{xz} and d_{yz} orbitals, which is the primary cause of the large quadrupole splittings. Hückel calculations[33] suggest that this result is fairly insensitive to changes in geometry and that large negative ΔE_Q values are not found for charge transfer (superoxide-like) configurations.

Table X also gives results for three semiempirical calculations on heme–CO in the collinear configuration. In each case the quadrupole splitting is smaller than in the corresponding oxygen complex, although only the Xα result is in good agreement with experiment. All calculations predict a positive principal EFG component oriented along the normal to the heme plane, in agreement with experiment;[44] the calculated anisotropy parameter (0.1) is, however, significantly smaller than the experimental estimates (0.4, 0.7).[44] The small Xα result arises from the nearly equal populations of the three t_{2g} orbitals and the small difference between the two e_g populations (see Table VI), suggesting that heme–CO is close to an idealized low-spin ferrous complex. By contrast, both the EHT and PPP calculations have a significant difference in the t_{2g} populations, as in the Fe–O_2 system. On the basis of extended Hückel calculations, Trautwein[44] has invoked a five-coordinate complex and an unusually short Fe–C bond distance to explain the Mössbauer spectrum. The Xα results given here suggest that such an extreme model is not necessary.

Table XI. Ground-State CI Coefficients

heme–O_2		heme–CO	
SCF	−0.901	SCF	0.937
Mainly Porphyrin $\pi\rightarrow\pi^*$			
13a″ → 14a″	−0.093	13a″ → 14a″	0.041
16a′ → 18a′	−0.069	15a′ → 17a′	−0.045
$(17a')^2 \rightarrow (18a')^2$	0.106	$(16a')^2 \rightarrow (14a'')^2$	−0.125
$(17a')^2 \rightarrow (14a'')^2$	0.098	$(16a')^2 \rightarrow (17a')^2$	−0.122
$(16a')^2 \rightarrow (18a')^2$	0.071	12a″16a′ → 14a″17a′	−0.115
$(13a'')^2 \rightarrow (14a'')^2$	0.061	11a″16a′ → 14a″17a′	−0.089
12a″17a′ → 14a″18a′	0.106	12a′16a′ → 17a′18a′	0.059
11a″17a′ → 14a″18a′	0.063	15a′13a″ → 14a″17a′	0.051
Mainly Iron and Axial Ligands			
13a″ → 15a″	0.063	8a″9a″ → $(15a'')^2$	0.057
13a″ → 16a″	0.056		
$(13a'')^2 \rightarrow$ 14a″15a″	−0.072		
$(13a'')^2 \rightarrow$ 14a″16a″	−0.058		
$(13a'')^2 \rightarrow (15a'')^2$	0.085		
$(13a'')^2 \rightarrow$ 15a″16a″	0.100		
$(13a'')^2 \rightarrow (16a'')^2$	0.071		
$(13a'')^2 \rightarrow$ 15a″17a″	−0.067		
$(13a'')^2 \rightarrow$ 16a″17a″	−0.073		

E. Ground State Correlation Effects. It has been pointed out before[8,35] that in the Hartree–Fock approximation the ground state of heme–O_2 is not a singlet; in fact the closed-shell SCF state that we have been discussing is not even the lowest singlet state in this approximation—there is an open-shell singlet of A″ symmetry which is lower in energy.[35] Since the true ground state of oxyhemoglobin is a singlet, electron correlation must play an essential role. (Recent magnetic susceptibility measurements[50] which were interpreted as implying that there exists a thermally populated triplet state have been challenged.[51] Also, the absorption spectrum of oxyhemoglobin changes little with temperature,[52] which suggests that spin mixing is unimportant.) The situation is much the same in ozone, where a $^3B_2$ state lies below the $^1A_1$ ground state in the Hartree–Fock approximation.[38] In ozone the closed-shell double excitation $(1a_2)^2 \rightarrow (2b_1)^2$ makes the most important correlation contribution to the $^1A_1$ state, lowering its energy below the $^3B_2$.[53] A similar effect occurs in heme–O_2. The dominant configurations from the single plus double CI ground state eigenvector are shown in Table XI. We note that several

single excitations are important, despite the fact that they cannot couple directly to the SCF configuration. The excitations from 13a″ to 15a″, 16a″, and 17a″ are FeO_2 $\pi \rightarrow \pi^*$ excitations roughly similar to the $1a_2 \rightarrow 2b_1$ orbitals in ozone (see Table III). The correlation energy of the configurations we have selected is 1.99 eV, enough to make this $^1A'$ state the lowest of all singlets and triplets.

In spite of the importance of correlation in the energies, we see from Table XI that the ground state is still dominated by the closed-shell SCF configuration, and hence that this still provides a useful description of the ground-state properties. Correlation effects make the iron slightly more positive (0.45 → 0.57) and the oxygen molecule more negative (0.06 → −0.09). Details of the iron populations are given in Table VI. The principal change is in the $3d_{xz}$ and $3d_{yz}$ orbitals which lose 0.08 and 0.05 electron, respectively. Most of this charge enters the $2p_x$ orbitals of O^2: the change in the O^1 $2p_x$ population is 1.27 → 1.33, while that for O^2 $2p_x$ is 1.14 → 1.24. This correlation excitation into the O_2 $\pi_g{}^a$ orbitals is analogous to excitations into the antibonding $2b_1$ orbital of ozone.

The effect of correlation on the Mössbauer parameters is shown in Table X. There is a change of about 0.3 mm/s in ΔE_q, but the qualitative behavior discussed above is unaltered.

Correlation effects are qualitatively less important in heme-CO, probably because of the high energy of the CO π^* orbitals. Even in the Hartree-Fock approximation the closed-shell state considered above is the lowest state of singlet or triplet symmetry. The configurations listed in Table XI show that, while the porphyrin correlation effects are nearly the same as in heme-O_2, significant contributions from the CO ligand are absent. The only axial configuration listed in the table involves the imidazole π system. This is another indication of the difference in electronic structure between heme-CO and heme-O_2.

IV. Excited States

For the purpose of theoretical discussion, it is convenient to divide the excited states of hemoglobins into a number of classes depending on the qualitative nature of the electron promotions involved. We shall be concerned here only with the transitions arising from the heme chromophore itself. Such bands are observable between 0.5 and 4.5 eV where there are no strong protein absorptions; higher energy transitions are masked by the protein. The most intense heme peaks are porphyrin $\pi \rightarrow \pi^*$ transitions. Small variations in these peaks occur in the different hemoglobins, but in the main they are independent of the state of axial ligation or oxidation. More variable are the weaker charge transfer transitions, which involve electron transfer to or from the central iron atom. Although it is difficult to make definite assignments, it appears likely that this type of transition is responsible for several observed peaks in oxyhemoglobin, as well as for the near-infrared transitions in deoxy- and methemoglobins. Another category of spectral transition involves the crystal field d-d bands, which are expected to be quite weak. Finally, there may be bands based primarily on transitions intrinsic to the axial ligand, some of which may occur at low enough energy to avoid being masked by protein absorption. In this section we discuss each of these types of transition for oxy- and carboxyhemoglobin and make comparisons with the available spectral data.

The locations of the spectral features of oxyhemoglobin are shown in Table XII. There are at least ten peaks that are currently thought to arise from electronic transitions; additional peaks appear to correspond to vibrationally excited bands of certain of these transitions (e.g., Q_v). The porphyrin $\pi \rightarrow \pi^*$ bands are labeled Q, B, and N in accordance with traditional nomenclature. The peaks labeled I–VII are those identified by Eaton et al. using a variety of approaches;[5] previous ex-

Table XII. Spectral Features of Oxyhemoglobin

	I	II	III	IV	Q	V	VI	B	N	VII
A. Experimental Results (from Ref 5)										
excitation energy, eV	0.95	1.08	1.26	1.59	2.22	2.28	2.73	2.99	3.60	3.84
oscillator strength			0.0026	0.0021	0.12		0.022	1.3	0.54	0.15
polarization			*x*	*yz*	*xy*		*z*	*xy*	*xy*	*z*
B. Assignments of Transitions										
Eaton et al.[a]	$d_{yz} \rightarrow d_{xz} + O_2\pi^*$	$d_{x^2-y^2} \rightarrow d_{xz} + O_2\pi^*$	$a_{2u} \rightarrow d_{xz} + O_2\pi^*$	$a_{1u} \rightarrow d_{xz} + O_2\pi^*$		$d \rightarrow d$	$d \rightarrow d$			$O_2\pi_u \rightarrow d_{xz} + O_2\pi^*$
Churg and Makinen[b]			$a_{2u}a_{1u} \rightarrow d_{xz} + O_2\pi^*$				a Q_v band and $a_{2u}a_{1u} \rightarrow d_{z^2}$			$a'_{2u} \rightarrow d_{z^2}$ and $b_{2u} \rightarrow d_{x^2-y^2}$
this paper[c]	$d_{yz} + O_2\pi^* \rightarrow d_{xz} + O_2\pi^*$	$d_{xz} + e_g \rightarrow d_{xz} + O_2\pi^*$ *or* $d_{xz} + e_g \rightarrow e_g^* + O_2\pi^*$ plus others	$a_{2u} \rightarrow d_{xz} + O_2\pi^*$ *or* $d_{xz} + e_g \rightarrow d_{xz} + O_2\pi^*$	$a_{1u} \rightarrow d_{xz} + O_2\pi^*$ *or* $d_{xz} + e_g \rightarrow d_{xz} + O_2\pi^*$		$d(^1A_{1g}) \rightarrow d(^1E_g)$	$d(^1A_{1g}) \rightarrow d(^1A_{2g})$ *or* $a_{2u} \rightarrow d_{z^2}$ *or* $d_{xz} + e_g \rightarrow lm$			$a'_{2u}b_{2u} \rightarrow d_{z^2}$ *or* Hartley-like band

[a] Reference 5. [b] Reference 6; the suggested transition at 1.9 eV is identified with d_{xz}, $d_{yz} \rightarrow e_g$. [c] For the 1.9-eV transition, a possible candidate from the PPP calculation is d_{xz}, $d_{yz} \rightarrow e_g$.

Table XIII. Spectral Features of Carboxyhemoglobin[a]

	I	Q	II	B	N
excitation energy, eV	1.98	2.2	2.21	2.96	3.6
oscillator strength		0.1		1.0	0.5
polarization		*xy*		*xy*	*xy*

[a] From ref 5.

Table XIV. Complete Single CI Results for Heme-O_2

	theory[a]			expt	
	excitation energy[b]	polarization[c]	osci strength	band	energy
1A″	−0.03	*x*	0.0	I	0.95
2A″	1.71	*x*	0.0001	II	1.08
3A″	1.80	*x*	0.0005	III	1.26
1A′	1.92	0.14	0.0002	IV	1.59
4A″	1.95	*x*	0.005		
5A″	2.04	*x*	0.041	Q	2.22
2A′	2.25	2.13	0.016		
6A″	2.47	*x*	0.0		
7A″	2.63	*x*	0.001		
3A′	2.86	*z*	0.08		
4A′	3.07		0.0		
5A′	3.35	0.12	0.346	V1[d]	2.73
8A″	3.37	*x*	0.0		
9A″	3.39	*x*	0.0002		
6A′	3.57	2.64	0.334	B	2.99
10A″	3.60	*x*	0.309		
11A″	3.77	*x*	0.018		
7A′	3.87	*y*	0.057		
8A′	3.92	*y*	0.107		
9A′	3.96	*y*	0.034	V	2.28
10A′	4.01	*y*	0.442	N	3.60
12A″	4.13	*x*	0.476		
13A″	4.18	*x*	0.0	V1[e]	2.73
11A′	4.36	0.30	0.045	VII	3.84
14A″	4.42	*x*	0.002		
15A″	4.58	*x*	0.0		
12A′	4.65	*y*	0.231		
16A″	4.66	*x*	0.0		
17A″	4.73	*x*	0.011		
18A″	4.74	*x*	0.248		
13A′	4.78	0.99	0.037		
19A″	4.79	*x*	0.473	L	
20A″	4.87	*x*	0.158		
14A′	4.88		0.0		
15A′	4.92	*y*	0.579	L	
16A′	5.05	*y*	0.002		

[a] The first four columns of the table are theoretical results. [b] Energies in eV. [c] The number indicates the *y* to *z* polarization ratio. [d] Possible assignment discussed in section IVB. [e] Possible assignment discussed in section IVC.

perimental work is reviewed by these authors. In oxymyoglobin[6] the polarization ratio has been used to suggest an additional spectral transition at 1.9 eV, although it is possible that a tail of one of the other *z*-polarized absorption bands is involved. Table XII also lists the assignments in terms of the dominant orbital contributions suggested for other than the porphyrin $\pi \rightarrow \pi^*$ oxyhemoglobin transitions by Eaton et al.,[5] Churg and Makinen,[6] and us. The spectrum of carboxyhemoglobin in the same frequency range is much simpler (see Table XIII). There are only five bands of which three correspond to the porphyrin $\pi \rightarrow \pi^*$ transitions (Q, B, N).

As suggested by Makinen and Eaton,[12] the difference between the oxy and carboxy spectrum can be used as a qualitative guide to the transitions directly involving the ligand. Additional information can be obtained, in principle, from comparison with the spectrum of the ferrous cyanide complex, although the recent single-crystal study[6] needs to be supplemented by CD and MCD measurements to better characterize the weak transitions. Making use of single-crystal polarization data and of CD and MCD measurements, Eaton et al.[5] have recently assigned the observed spectral features and related them to transitions found in the extended Hückel calculation referred to in earlier sections of this paper. Different assignments have been given for some of the transitions by Churg and Makinen.[6] In what follows, we present assignments in accord with the PPP and/or Xα results and indicate whether they agree or disagree with the works of Eaton et al.[5] and Churg and Makinen.[6]

Table XV. Complete Single CI Results for Heme-CO[a]

	theory			expt	
	excitation energy	polarization	osci strength	band	energy
1A″	2.07	*x*	0.0		
1A′	2.21	*y*	0.03	Q	2.18
2A″	2.21	*x*	0.02		
3A″	2.21	*x*	0.014		
2A′	2.26	*y*	0.001		
3A′	3.32		0.0		
4A″	3.33	*x*	0.0		
4A′	3.38		0.0		
5A′	3.65	*y*	0.43	B	2.96
5A″	3.66	*x*	0.43		
6A″	3.73	*x*	0.0005		
6A′	3.75	*y*	0.0	I	1.98
7A″	3.77	*x*	0.0		
7A′	3.84	*y*	0.0008		
8A″	4.01	*x*	0.0006		
8A′	4.09	6.24	0.23	N	3.60
9A′	4.11	*y*	0.44		
9A″	4.12	*x*	0.003		
10A″	4.12	*x*	0.79		
10A′	4.28		0.0		
11A″	4.35	*x*	0.0	II	2.36
11A′	4.41	0.28	0.12		
12A″	4.48	*x*	0.0		
13A″	4.59	*x*	0.0002		
12A′	4.64	*y*	0.002		
14A″	4.61	*x*	0.0		
15A″	4.67	*x*	0.001		
16A″	4.86	*x*	0.56	L	
13A′	4.87	*y*	0.61		

[a] See footnotes to Table XIV.

The PPP results for complete single CI calculations on heme-O_2 and heme-CO are given in Tables XIV and XV; both tables give calculated excitation energies, polarizations, and oscillator strengths and certain experimental assignments (see also Table XII). Table XVI lists the dominant configurations that contribute to each of the state vectors. As one might expect, the number of calculated transitions is greater than the number of observed peaks. Our reasons for making the assignments shown in these tables are given below.

In the present version of the Xα method we can determine the energies of excited states only if they are well represented as single-electron promotions from a closed-shell configuration. For such a case a Slater transition state may be calculated which involves transfer of half an electron from the donor or acceptor orbital; the difference in one-electron energies of the two orbitals is a good approximation to the average of the singlet and triplet excitation energies. If configuration interaction is important in the excited states this method yields the average transition energy of the states that mix. In Figure 4 we show the energy levels for the ground state of heme-O_2 and for three transition states that are candidates for the absorption peaks in Table XII.

Table XVI. Coefficient for Complete Single CI Calculation[a,b]

state	contributing configurations
	(I) HbO_2
	(a) A′ Symmetry
1A′	0.6418(13a″ → 14a″) + 0.6761(16a′ → 18a′)
2A′	−0.7835(17a′ → 18a′) − 0.5213(12a″ → 14a″)
3A′	0.7307(13a″ → 14a″) − 0.5737(16a′ → 18a′)
4A′	0.9749(14a′ → 18a′)
5A′	0.8819(13a″ → 15a″) + 0.3007(12a″ → 14a″)
6A′	−0.6706(12a″ → 14a″) + 0.3087(13a″ → 15a″) +0.3030(11a″ → 14a″) + 0.3124(16a′ → 19a′) + 0.2517(17a′ → 18a′) + 0.2542(12a″ → 15a″) − 0.2483(15a′ → 18a′)
7A′	0.7597(17a′ → 19a′) + 0.2019(11a″ → 14a″) − 0.2744(10a″ → 14a″) − 0.2660(15a′ → 19a′)
8A′	−0.4338(12a″ → 15a″) + 0.4502(11a″ → 14a″) + 0.4034(16a′ → 24a′) + 0.3673(16a′ → 19a′) − 0.2168(17a′ → 18a′) − 0.2512(17a′ → 19a′)
9A′	0.6826(16a′ → 24a′) + 0.3770(12a″ → 15a″) − 0.2193(11a″ → 14a″) + 0.2183(11a′ → 24a′) + 0.2201(13a′ → 24a′)
10A′	0.6968(12a″ → 15a″) − 0.3095(17a′ → 18a′) + 0.2389(12a″ → 14a″) + 0.2562(11a″ → 14a″) + 0.2310(16a′ → 19a′) + 0.2074(12a″ → 16a″) + 0.2609(13a″ → 18a″)
11A′	−0.8016(13a″ → 16a″) + 0.2507(16a′ → 18a′) − 0.2138(17a′ → 19a′) − 0.2043(10a″ → 14a″) + 0.2642(13a″ → 17a″)
12A′	−0.6582(11a″ → 14a″) + 0.6588(16a′ → 19a′)
13A′	−0.5474(10a″ → 14a″) − 0.4305(17a′ → 19a′) + 0.3092(13a″ → 16a″) − 0.3307(13a′ → 18a′) − 0.2646(9a″ → 14a″) + 0.2631(12a′ → 18a′) − 0.2217(15a′ → 19a′)
14A′	0.9240(14a′ → 24a′)
15A′	0.6977(15a′ → 18a′) + 0.3301(12a″ → 16a″) + 0.3906(13a″ → 18a″) − 0.2219(12a″ → 15a″)
16A′	−0.7321(13a″ → 17a″) + 0.3817(12a″ → 16a″) − 0.2604(13a″ → 16a″) − 0.2291(9a″ → 14a″)
	(b) A″ Symmetry
1A″	−0.3517(11a′ → 14a″) + 0.3370(11a′ → 15a″) + 0.2901(16a′ → 14a″) − 0.2949(16a′ → 15a″) − 0.2401(16a′ → 16a″) − 0.2562(12a′ → 14a″) + 0.2038(13a′ → 14a″) + 0.2695(12a′ → 15a″) − 0.2149(13a′ → 15a″) + 0.2320(12a′ → 16a″) + 0.2877(11a′ → 16a″)
2A″	0.7070(16a′ → 14a″) + 0.4786(13a″ → 18a′) + 0.3172(16a′ → 15a″) + 0.2543(16a′ → 16a″)
3A″	−0.7512(13a″ → 18a′) + 0.5380(16a′ → 14a″)
4A″	0.5130(16a′ → 15a″) − 0.3709(13a″ → 18a′) − 0.3072(17a′ → 14a″) + 0.3573(16a′ → 16a″) − 0.2096(11a′ → 14a″) + 0.2785(11a′ → 15a″) + 0.2334(11a′ → 16a″)
5A″	0.7912(17a′ → 14a″) − 0.3168(12a″ → 18a′) − 0.2022(17a′ → 15a″)
6A″	−0.6581(14a′ → 15a″) − 0.5830(14a′ → 16a″) + 0.3791(14a′ → 17a″)
7A″	−0.8485(17a′ → 15a″) + 0.3331(12a″ → 18a′) −0.2798(17a′ → 16a″)
8A″	0.9691(14a′ → 14a″)
9A″	0.6554(16a′ → 15a″) + 0.5142(16a′ → 17a″) − 0.4646(16a′ → 16a″)
10A″	−0.6795(12a″ → 18a′) + 0.3742(17a′ → 16a″) − 0.3519(17a′ → 15a″) − 0.2228(17a′ → 14a″) − 0.2364(17a′ → 17a″) + 0.2478(15a′ → 14a″)
11A″	0.6021(17a′ → 16a″) + 0.3649(11a″ → 18a′) + 0.3057(12a″ → 18a′) + 0.3426(13a″ → 19a′) − 0.3262(17a′ → 17a″) − 0.2227(17a′ → 15a″) − 0.2718(15a′ → 16a″)
12A″	−0.5499(13a″ → 19a′) − 0.4046(11a″ → 18a′) + 0.4223(16a′ → 18a″) + 0.2874(17a′ → 14a″) + 0.2170(12a″ → 18a′) + 0.3835(17a′ → 16a″)
13A″	0.9998(14a′ → 22a″)
14A″	0.5433(10a″ → 18a′) − 0.4372(11a″ → 19a′) + 0.3890(13a′ → 14a″) − 0.3067(12a′ → 14a″) + 0.2804(9a″ → 18a′)
15A″	−0.6797(17a′ → 18a″) + 0.6110(12a″ → 19a′)
16A″	−0.7179(14a′ → 15a″) − 0.5730(14a′ → 17a″) + 0.3684(14a′ → 16a″)
17A″	0.7541(13a″ → 24a′) − 0.3177(13a″ → 19a′) + 0.3057(11a″ → 18a′) + 0.2031(13a″ → 25a′)
18A″	−0.6368(11a″ → 18a′) + 0.5285(13a″ → 19a′) + 0.3515(13a″ → 24a′) − 0.2638(15a′ → 14a″)
19A″	0.6731(15a′ → 14a″) + 0.4153(17a′ → 17a″) + 0.2509(12a″ → 18a′) + 0.2968(17a′ → 16a″) + 0.2756(13a″ → 19a′)
20A″	0.7224(17a′ → 17a″) − 0.4379(15a′ → 14a″) + 0.3412(17a′ → 16a″) + 0.2217(16a′ → 22a″)
	(II) HbCO
	(a) A′ Symmetry
1A′	−0.8060(16a′ → 17a′) − 0.4472(12a″ → 14a″)
2A′	0.6770(13a″ → 14a″) + 0.6579(15a′ → 17a′)
3A′	0.9714(13a′ → 17a′) − 0.2177(13a′ → 20a′)
4A′	−0.6393(13a″ → 14a″) + 0.6829(15a′ → 17a′)
5A′	0.7456(12a″ → 14a″) − 0.3415(11a″ → 14a″) − 0.3134(14a′ → 17a′) − 0.2755(16a′ → 17a′) − 0.2471(15a′ → 18a′)
6A′	−0.7771(15a′ → 24a′) + 0.2756(15a′ → 21a′) + 0.4702(11a′ → 24a′)
7A′	0.8697(16a′ → 18a′) + 0.2024(11a′ → 17a′) + 0.2471(14a′ → 18a′)
8A′	0.4526(13a″ → 15a″) + 0.3741(11a″ → 14a″) + 0.3120(15a′ → 18a′) − 0.3338(15a′ → 19a′) − 0.3272(13a″ → 16a″) − 0.2787(13a″ → 18a″) − 0.2347(16a′ → 17a′)
9A′	0.4524(11a″ → 14a″) − 0.3177(16a′ → 17a′) + 0.2309(12a″ → 14a″) − 0.2600(13a″ → 15a″) + 0.3723(15a′ → 18a′) + 0.3259(15a′ → 19a′) + 0.2743(13a″ → 16a″) + 0.2080(13a″ → 17a″) + 0.2757(13a″ → 18a″)
10A′	−0.9352(13a′ → 24a′) + 0.3211(13a′ → 21a′)
11A′	−0.6989(13a″ → 15a″) − 0.4461(15a′ → 19a′) − 0.3587(13a″ → 18a″) − 0.2017(12a″ → 15a″)
12A′	0.9515(16a′ → 19a′)
13A′	0.5514(11a″ → 14a″) − 0.3999(15a′ → 18a′) − 0.6442(14a′ → 17a′)
	(b) A″ Symmetry
1A″	0.8245(13a″ → 17a′) + 0.4914(15a′ → 14a″)
2A″	−0.6319(16a′ → 14a″) − 0.4860(15a′ → 14a″) + 0.4294(12a″ → 17a′) + 0.2716(13a″ → 17a′)
3A″	0.6529(15a′ → 14a″) − 0.5126(16a′ → 14a″) − 0.3806(13a″ → 17a′) + 0.2418(12a″ → 17a′)
4A″	−0.9676(13a′ → 14a″) + 0.2238(13a′ → 19a″)
5A″	−0.7317(12a″ → 17a′) − 0.3657(11a″ → 17a′) − 0.3197(14a′ → 14a″) − 0.2640(16a′ → 14a″) − 0.2674(13a″ → 18a′)
6A″	−0.9177(16a′ → 15a″) + 0.3205(16a′ →16a″)
7A″	−0.7727(13a″ → 24a′) + 0.2761(13a″ → 21a′) + 0.2032(9a″ → 24a′) + 0.2490(10a″ → 24a′) − 0.2782(8a″ → 24a′)
8A″	−0.4948(15a′ → 15a″) + 0.4963(15a′ → 18a″) + 0.4920(15a′ → 16a″) + 0.3172(13a″ → 19a′) − 0.2054(11a′ → 18a″)
9A″	0.8202(13a″ → 19a′) + 0.2671(15a′ → 15a″)
10A″	−0.5644(11a″ → 17a′) + 0.4154(16a′ → 14a″) − 0.4783(13a″ → 18a′) + 0.3032(12a″ → 17a′) + 0.2800(15a′ → 17a″)
11A″	(13a′ → 22a″)

Table XVI (*Continued*)

state	contributing configurations	state	contributing configurations
12A″	0.6525(15a′ → 15a″) + 0.5389(15a′ → 18a″) + 0.2011(11a′ → 14a″) + 0.2085(15a′ → 19a″) − 0.2104(11a′ → 18a″)	14A	−0.5367(16a′ → 17a″) + 0.4906(12a″ → 18a′) + 0.3832(11a′ → 14a″) + 0.2433(10a″ → 17a′) + 0.2911(11a″ → 18a′)
13A″	0.4162(16a′ → 17a″) − 0.4065(12a″ → 18a′) + 0.3297(10a″ → 17a′) + 0.3077(9a″ → 17a′) + 0.3402(11a″ → 18a′) − 0.2223(15a′ → 15a″) − 0.2182(15a′ → 18a″) + 0.2508(11a′ → 14a″) − 0.2447(8a″ → 17a′)	15A″	−0.6492(16a′ → 16a″) − 0.6531(16a′ → 18a″) − 0.2470(16a′ → 15a″)
		16A″	0.5949(11a″ → 17a′) − 0.4750(13a″ → 18a′) − 0.5623(14a′ → 14a″)

[a] All coefficients greater than 0.2 are listed. [b] For orbital labels see Tables III and IV.

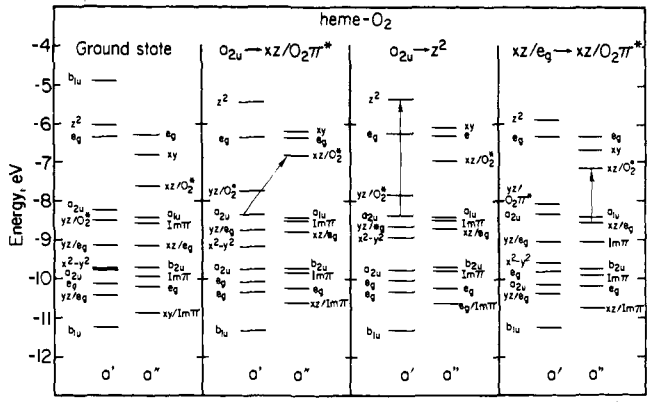

Figure 4. Xα transition-state calculations for heme–O_2. Orbitals involved in the transition are connected by an arrow.

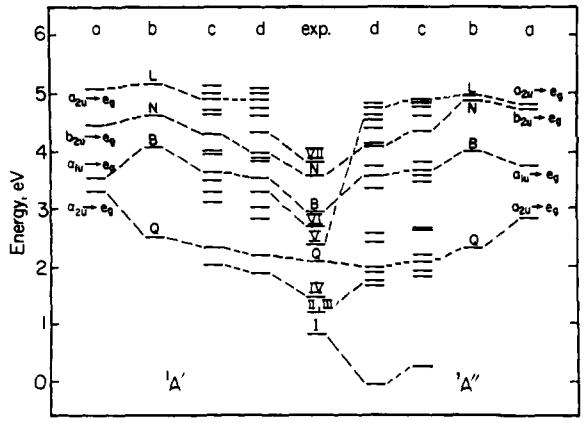

Figure 5. PPP single-excitation CI results for heme–O_2. Column (a) gives molecular orbital promotions (no CI); column (b) includes CI among these four states; column (c) includes excitations among those orbitals starred in Table III; column (d) is a complete single-excitation CI. Experimental values are from ref 5. Dashed lines indicate suggested assignments as discussed in the text.

A. Porphyrin $\pi \rightarrow \pi^*$ Transitions. The Q, B, N, and L peaks characteristic of all metalloporphyrins arise from $\pi \rightarrow \pi^*$ transitions centered primarily on the porphyrin ring. These features can be rationalized in terms of the "six-orbital" model of closed-shell metalloporphyrins,[20] which is illustrated in columns a and b of Figure 5. The one-electron promotions $a_{1u} \rightarrow e_g$ and $a_{2u} \rightarrow e_g$ are mixed strongly by the electron interaction, with the result that the transition dipoles of these excitations add to produce the intense Soret (B) band, and nearly cancel to produce the much weaker visible (Q_0) band; the Q_v band is apparently a vibrationally induced mixture of the same electronic transition.[54] The higher energy N and L bands are derived in much the same way from the promotions $b_{2u} \rightarrow e_g$, $a_{2u}' \rightarrow e_g$;[20] the L band is obscured in heme proteins by absorption of aromatic side chains. The three bands that can be seen are nearly identical in oxy- and carboxyhemoglobin (see Tables XII and XIII).

The energies shown in Figure 5 are based on PPP single CI calculations on heme–O_2; the $\pi \rightarrow \pi^*$ results for heme–CO are very similar. As more configurations are added beyond the six-orbital model (columns c and d), the excitation energies continue to decrease, coming into closer agreement with experiment. The excited state wave functions, however, are still qualitatively in accord with the simple model. For example, in heme–CO the y component of the Q band, Q_y, has the following wave function in the complete single CI calculation (Table XVI):

$$0.806(a_{2u} \rightarrow e_g{}^*y) + 0.447(a_{1u} \rightarrow e_g{}^*x) + \ldots$$

where $e_g{}^*y$ and $e_g{}^*x$ are the two components of the degenerate unoccupied orbital. Upon inclusion of doubly excited configurations this vector is little changed:

$$0.768(a_{2u} \rightarrow e_g{}^*y) + 0.491(a_{1u} \rightarrow e_g{}^*x) + \ldots$$

The excitation energy, however, is changed from 2.2 to 3.0 eV upon going to the double-CI calculation. This change comes about because in the latter calculation electron correlation is better represented in the ground state than in the excited states. As we discussed in section IIIE, the dominant correlation contributions come from closed-shell type double excitations; in the excited states such contributions represent *triple* excitations from the SCF reference configuration, and hence are not included in the wave function expansion. PPP calculations on polyenes have demonstrated that this imbalance can be removed by approximate procedures or doing more extensive CI;[55] the simplest approximation is to use as excitation energies the difference between the CI energy of the excited states and the energy of the HF ground state. In the present case, this yields an excitation energy for the Q band of 1.5 eV, apparently overcorrecting for the correlation energy difference between the ground and excited states.

It should be noted that the excited-state eigenvectors do not always have the simple form illustrated above. In heme–CO the x component of the Q state has the following more complicated representation in the single CI calculation (Table XVI):

$$0.632(a_{2u} \rightarrow e_g{}^*x) - 0.429(a_{1u} \rightarrow e_g{}^*y) + 0.486(e_g/yz \rightarrow e_g{}^*x) - 0.272(e_g/xz \rightarrow e_g{}^*y) + \ldots$$

where the occupied orbital in the third and fourth contributing configuration is about 40% on iron 3d and 60% in the porphyrin π system (15a′ and 13a″ in Table IV). The simpler form for Q_y may result from the fact that it corresponds to excitation

to the lowest state of A′ symmetry, while Q_x involves the second state of A″ symmetry; similar results are found for heme-O_2 (see Table XIV). When doubly excited configurations are added, the eigenvector for Q_x simplifies to

$$0.76(a_{2u} \rightarrow e_g^*x) - 0.499(a_{1u} \rightarrow e_g^*y) + \ldots$$

which is in close correspondence with the y component. This demonstrates that the amount of mixing that takes place in the $\pi \rightarrow \pi^*$ excited states is sensitive to the size of the CI matrix. It is unwise, therefore, to attach too much significance to the detailed character of the excited-state vectors for such a complicated system. Nevertheless, the gross features of the porphyrin transitions are independent of the size of the CI or of the nature of the axial ligand, and are in good accord with the six-orbital model. This model uses 15a′, 17a′, 18a′, 11a″, 12a″, and 14a″ in heme-O_2 and 14a′, 16a′, 17a′, 11a″, 12a″, and 14a″ in heme-CO (see Tables III, IV, and XVI). In addition to these, the B and N bands in heme-O_2 in the single CI approximation have smaller contributions from 11a″, 18a″ (b_{1u}, porphyrin π), from 19a′ (b_{2u}, porphyrin π), and from 15a″, 16a″ (imidazole and FeO_2 π orbitals). These serve to lower the excitation energies relative to the six-orbital model (see Figure 5), but do not greatly change the relative energies or qualitative interpretation. The calculated splitting between the Q and B bands is about 0.5 eV higher than the experimental result; similar behavior has been seen in previous PPP calculations on porphyrins.[20] The calculated N and L band positions are about 0.5 and 1.3 eV above the Soret band, in good agreement with the values of 0.6 and 1.5 eV seen in many metalloporphyrins.[20]

The porphyrin transitions can easily be identified in Tables XIV and XV by their large calculated oscillator strengths. The calculated values are not quantitatively accurate—for example, they make the N band more intense than the B band—but they do give a correct qualitative picture. Although there are other porphyrin transitions in the region below 5 eV, none of them are calculated to have sufficient oscillator strengths to be observed.

It is of interest that the strong B and N transitions in HbO_2 (see Table XIV) are calculated to have nearly equal contributions from x and y polarized components, while the Q band is calculated to have unequal intensities for the two components. This is in agreement with the experimental results of Eaton and Makinen.[12] The apparently greater sensitivity to reduction in symmetry of the Q transition, relative to B and N, has been rationalized[54] in terms of the cancellations in the $a_{1u}, a_{2u} \rightarrow e_g^*$ excitations that yield the reduced intensity of this band (see above).

The description of porphyrin transitions found here is very similar to that of earlier studies on model porphyrin complexes.[20,56] The axial ligands have little effect on the energies or strengths of the transitions (compare Tables XIV and XV). Inclusion of doubly excited configurations appears to alter the quantitative results, but additional calculations are required for a definitive conclusion.

We discussed the Xα theory of porphyrin transitions in earlier work on the copper complex.[26] The one-electron energy difference between the a_{1u}, a_{2u} and e_g^* orbitals is 2.0 eV for both heme-CO and heme-O_2 (see Figures 2 and 3) and is expected to represent the average of the singlets and triplets that form the Q and B bands. The experimental value for this average is 2.2 eV.[32] The splitting between the Q and B bands, caused by electron interaction, is not at present accessible to calculation by the Xα method. Similarly, the average of the N and L states should correspond to the $a_{2u}', b_{2u} \rightarrow e_g^*$ one-electron energy difference. The Xα value is 3.5 eV; the experimental value is unknown because the triplet states have not been identified. If we assume that these are 0.8 eV below the corresponding singlets (as for the Q band[32]), the experimental value is 3.8 eV. Hence the Xα method appears to give accurate results for the appropriate averages of the porphyrin transitions.

In some papers,[57] the correspondence of the porphyrin transitions in low-spin ferrous and ferric compounds (e.g., hemoglobin-O_2 and alkaline ferric hemoglobin) has been used to suggest that HbO_2 has a ferric iron and that the superoxide structure is appropriate. Although other arguments against this formulation of the ground state have been given above, it is important to emphasize here that the essential identity of the porphyrin transitions in HbO_2 and MbCO (Tables XIV and XV; Q, B, N), with the latter certainly having an $Fe^{2+}CO$ moiety, shows that the ferrous/ferric comparison is not meaningful. The only valid conclusion is that the porphyrin transitions are relatively insensitive to the sixth ligand. Also, of interest in this regard is the fact that the iron in MbO_2[14] is apparently 0.3 Å out of the porphyrin plane on the proximal side, while in HbCO the iron is essentially in the porphyrin plane.[58]

B. Charge-Transfer Transitions. We have pointed out earlier that calculating charge-transfer transitions is difficult because the results depend so heavily on the relative positions of the metal 3d and the ligand π orbitals.[26] This relative ordering is, in turn, very sensitive to the method of calculation; in particular, the PPP and Xα methods have been shown to give different results. Within the extended Hückel method, alternative methods of choosing ionization potentials can also lead to a significant variation in transition energies.[32] In spite of these difficulties it is important to examine theoretically the possible contribution of charge-transfer transition to the observed spectra.

There are three factors that simplify the problem of identifying the transitions in oxyhemoglobin: (1) Certain bands in oxyhemoglobin appear not to have analogues in carboxyhemoglobin (see Tables XII and XIII). (2) Bands III and IV in oxyhemoglobin exhibit significant magnetic circular dichroism.[5] (3) The observed near-infrared bands are low enough in energy so that there are only a small number of possible assignments, even allowing for systematic errors in the orbital energies.

The separation of the broad 1.5-eV band in HbO_2, the near-infrared band characteristic of oxyhemoglobin,[11] into two components (III and IV) was deduced by Eaton et al.[5] on the basis of the change in polarization across the band and on the existence of two peaks in the magnetic circular dichroism spectrum. Following extended Hückel calculations, these authors postulated that the transitions from the a_{1u}, a_{2u} orbitals to the lowest unoccupied orbital, $d_{xz}/O_2\pi^*$, are responsible for the observed absorption (see Table XII). As already described (section IIIA), a low-lying orbital of this type occurs in all of the calculations for the oxygen ligand; the corresponding orbital for carbon monoxide is much higher in energy. The Xα transition state calculation for $a_{2u} \rightarrow d_{xz}/O_2\pi^*$ is shown in the second column of Figure 4. Orbitals involving oxygen and iron have risen in energy relative to the ground state by ~1 eV because extra charge has been transferred to these atoms. The a_{2u} porphyrin π orbital is sufficiently delocalized that removal of half an electron changes its energy by only a small amount, ~0.1 eV. The calculated excitation energy of this transition is 1.56 eV. A similar calculation on the $a_{1u} \rightarrow d_{xz}/O_2\pi^*$ transition (not shown in the figure) yields 1.67 eV. These energies are so close that they might not be resolved as separate bands. The calculations predict that the low-frequency side of the band should be x polarized and the high-frequency side yz polarized in agreement with experiment;[5] the single-crystal measurements of Chung and Makinen on MbO_2[6] indicate that the z-polarized contribution is smaller than that calculated here (Table XIV). The assignment is in quantitative accord with the observed MCD spectrum.[5]

Other possible choices for bands III and IV are the transitions $xz/\text{eg} \rightarrow xz/O_2\pi^*$ and $yz/\text{eg} \rightarrow xz/O_2\pi^*$ (see Table XII). Column 4 of Figure 4 shows a transition-state calculation for the former promotion, which yields an energy difference of 2.23 eV. This is larger than the observed value of ~1.4 eV, but not outside the error limits of the calculation.

The PPP single excitation results yield bands that can be assigned to III and IV of a somewhat different and more complex form than the Xα description outlined above. Table XIV shows several singlet states with excitation energies below the Q band. The most likely candidates for bands III and IV have the following wave functions (Table XVI):

$$2A'': 0.707(16a' \rightarrow 14a'') + 0.479(13a'' \rightarrow 18a') + 0.317(16a' \rightarrow 15a'') + 0.254(16a' \rightarrow 16a'')$$

$$3A'': 0.751(13a'' \rightarrow 18a') - 0.538(16a' \rightarrow 14a'') + \ldots$$

$$1A': 0.642(13a'' \rightarrow 14a'') + 0.676(16a' \rightarrow 18a') + \ldots$$

In each case these involve excitations out of the $xz,yz/e_g$ occupied orbitals (16a′, 13a″) into the e_g^* porphyrin π orbitals (18a′, 14a″). Since these arise from g→g transitions in D_{4h} they have very little intensity, and furthermore involve the oxygen ligand only slightly in orbitals 14a″–16a″. In the Xα model, such transitions fall at much higher energy, greater than 3 eV (see Figure 2). Hence at the single CI level the PPP calculations do not appear to be in good accord either with experiment or with the Xα calculations.

When doubly excited configurations are included, however, excitations involving oxygen orbitals mix more prominently into the states below the Q band. The 2A″ state in the double CI calculation has the form

$$-0.499(16a' \rightarrow 14a'') - 0.372(17a' \rightarrow 14a'') - 0.268(11a' \rightarrow 14a'') + 0.244(17a' \rightarrow 15a'') + 0.224(11a' \rightarrow 15a'')$$
$$+0.195(12a' \rightarrow 15a'') + 0.188(11a' \rightarrow 16a'') + 0.160(12a' \rightarrow 16a'') + \ldots$$

Orbitals 11a′, 12a′, 14a″, 15a″, and 16a″ have substantial oxygen character (see Table III). A population analysis of this state indicates that, compared to the ground state, 0.18 electrons have been transferred out of the iron d_{yz} orbital into the d_{xz} orbital; at the same time 0.28 electrons have left the p_y and p_z orbitals of O^1 and O^2, most (0.21) of them entering the $2p_x$ orbitals of these atoms. The excited wave function thus corresponds to a 5π state[8] in which in-plane electrons in the FeO_2 units have been transferred to out-of-plane orbitals. This, then, is a candidate for band III. It is like the Xα transition ($a_{2u} \rightarrow xz/O_2\pi^*$) in that electrons enter the π orbitals of the FeO_2 unit, but unlike it in that there is no net charge transfer from the porphyrin.

The change in the 1A′ state upon going from single to double CI is not as large. In the double CI calculation the wave function becomes

$$0.615(13a'' \rightarrow 14a'') - 0.505(16a' \rightarrow 18a') - 0.163(13a'' \rightarrow 16a'') - 0.112(13a'' \rightarrow 15a'') + 0.128(13a'' \rightarrow 17a'') + 0.127(12a' \rightarrow 18a') + \ldots$$

Once again we have the greater involvement of orbitals with a large amount of oxygen character (12a′, 15a″, 16a″, 17a″), but the dominant characteristic of charge transfer from iron to porphyrin remains as in the single CI calculation. We have noted in earlier studies on CuPor[26] that Xα and PPP calculations differ in their predictions of charge-transfer transitions. In the Xα model, reduction of the metal occurs at energies several electron volts lower than is predicted by the PPP calculations; similarly, oxidation of the metal is more difficult in the Xα method than in the PPP. We see analogous results here, as the low-energy Xα transitions involve reduction of the iron. In copper porphine there is evidence to support the Xα description; for iron complexes the situation is less clear and may not be resolved until a more precise understanding of the nature of the excited states becomes available. There are indications from atomic calculations that the local exchange approximation underestimates the energy required to add an extra d electron to a metal.[59] Determination of the resulting error in metal complexes will require a more precise knowledge of the nature of the excited states.

Another candidate for a charge-transfer transition in HbO_2 is the moderately intense band at 2.7 eV (band VI of Table XII). One possible assignment is $a_{2u} \rightarrow a_{1g}(d_{z^2})$ as suggested by Churg and Makinen;[6] similar bands are seen near this energy (1.8 eV) in low-spin cytochromes.[60] An Xα transition state is shown in Figure 4 and gives an energy of 2.0 eV, in good agreement with the observed value. The corresponding transition should be present in carboxyhemoglobin, but if its energy were slightly higher it might be obscured by porphyrin Soret absorption, although no *z*-polarized intensity has been observed in this region.[6] The excitation $a_{2u} \rightarrow a_{1g}(d_{z^2})$ is electric dipole allowed even in the full D_{4h} point group, and this may help to explain the large oscillator strength of this charge-transfer band. Alternatively, band VI may be a d–d transition (see below) that has gained intensity through vibronic borrowing.[5] Another suggestion has been made by Churg and Makinen,[6] who argue that this region may contain vibronically induced intensity arising from the Q band.

The PPP results are very different from the Xα values because such a reduction of the metal (e.g., transitions of the form $a_{2u} \rightarrow d_{z^2}$, etc.) only occurs for energies greater than 5 eV in this model. The state in Table XIV that seems most likely to correspond to band VI is 5A′, since this is an intense transition that is nearly *z* polarized. Its wave function has the form (Table XVI)

$$0.882(13a'' \rightarrow 15a'') + 0.301(12a'' \rightarrow 14a'') + \ldots$$

The most significant charge transfer appears in the excitation into 15a″, which has the effect of reducing the imidazole. Such a transition might be sensitive to the assumed geometry, since if the imidazole is rotated its orbitals will no longer mix in the same way with the π orbitals of the FeO_2 unit.

Recently, Churg and Makinen have reported single-crystal spectra of the ferrous cyanide complex of myoglobin which exhibits *z*-polarized transitions similar to bands VI and VII in oxyhemoglobin.[6] If these bands indeed have the same origins, then band VII could not arise from the ozone-like transition discussed below (see Table XII). An alternative possibility[6] is an excitation from the lower lying porphyrin π orbitals a_{2u}', b_{2u} to $Fe(d_{z^2})$. The energy of such a state can be estimated from column 3 of Figure 4 to be 4.6 eV; this is in fair agreement with the observed value (3.84 eV).

C. Iron d–d Transitions. The first identification of possible d–d transitions in transition metal porphyrin compounds was made by Eaton and Charney[60] on the basis of features in the natural circular dichroism spectrum. In analyzing CD results, it is useful to compare the observed rotational strength with the dipole strength measured in the absorption spectrum. The rotational strength R is defined as the scalar product $\boldsymbol{\mu}\cdot\mathbf{m}$ of the magnetic and electric transition dipoles, while the dipole strength D is related to $|\mu|^2$. The ratio is the anisotropy or dissymmetry factor, defined as

$$g = \int \frac{A_L - A_R}{A} d\omega \approx \frac{4R}{D} = \frac{4\boldsymbol{\mu}\cdot\mathbf{m}}{|\boldsymbol{\mu}|^2}$$

where A_L, A_R, and A are the absorbance values for left, right, and unpolarized light. Figure 6 shows the singlet states of a

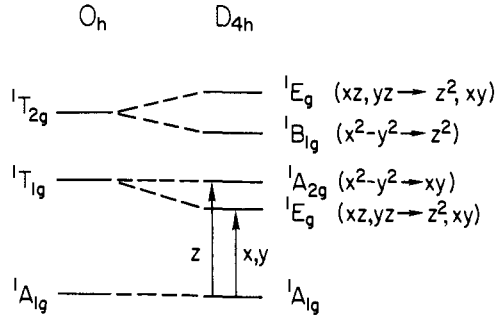

Figure 6. Ligand field diagram for a d^6 ion in a tetragonal field, from ref 59. Transitions shown are magnetic dipole allowed.

low-spin d^6 ion in a tetragonal ligand field along with their octahedral parentage.[60,61] The transitions $^1A_{1g} \rightarrow {}^1T_{1g}$ are magnetic dipole allowed (as indicated in the figure), but electric dipole forbidden. If these transitions become weakly electric dipole allowed by borrowing intensity from allowed transitions, they are expected to exhibit large anisotropy factors.

Two such bands are seen in the CD spectrum of carboxyhemoglobin at 2.0 and 2.2 eV (see I and II, Table XIII); they are, in fact, the only bands, other than porphyrin transitions, observed in the CO compound. Reasoning from Figure 6, Eaton et al.[5] have identified these bands with transitions to the $^1A_{2g}$ and ^1E_g crystal field states, respectively. The suggested ordering of the states is the opposite of the typical case shown in Figure 6; however, the short Fe-C bond (~1.77 Å) would tend to make the axial field stronger than the equatorial one, corresponding to Dt < 0 in the notation of Ballhausen and Moffitt[61] and a reversal of the two states. By a similar argument bands V and VI in oxyhemoglobin (Table XII) have been assigned by Eaton et al.[5] to the same pair of states. This implies that the crystal field splittings are larger for the oxygen ligand, which could be due to a very short Fe-O bond (1.75 Å), such as is found in a model complex.[13] In the oxy case, the polarization data do not suggest a relative ordering for the $^1A_{2g}$ and ^1E_d levels.

It is important to determine if these tentative assignments (2.28 and 2.73 eV in oxy, 1.98 eV ($^1A_{2g}$) and 2.22 eV (^1E_g) in carboxy) are supported by the various theoretical calculations. The extended Hückel calculations of Eaton et al.[5] yield values for these transitions at 3.84 ($^1A_{2g}$) and 4.09 eV (^1E_g) in oxy and 3.16 ($^1A_{2g}$) and 3.60 eV (^1E_g) in carboxy; for both ligands, the two ^1E_g components have very similar energies.

In the current parametrization of the PPP method, the d-d transitions in heme-O_2 (Table XIV) are 9A′ and 17A″ corresponding to ^1E_g, 13A″ corresponding to $^1A_{2g}$, and 14A′ corresponding to $^1B_{1g}$. The corresponding states in heme-CO (Tables XV) are 6A′, 7A″, 11A″, and 10A′, respectively. In heme-CO, the two ^1E_g components are nearly degenerate (3.75, 3.77 eV) and the $^1A_{2g}$ energy is 4.35 eV. For heme-O_2, there is a much larger splitting of the ^1E_g levels (3.96, 4.73 eV) and the $^1A_{2g}$ level is at 4.18 eV. The $^1B_{1g}$ crystal field state is predicted to be 0.7 eV above the $^1A_{2g}$ state in heme-O_2 and nearly degenerate with it in heme-CO; since this state is inaccessible from the ground state by either electric or magnetic dipole transitions, it should be very difficult to observe.

From the Xα results, the splitting of the $d_{x^2-y^2}$ and d_{xy} orbitals, which determines the excitation energy of the $^1A_{2g}$ state, is 2.9 eV for both heme-O_2 and heme-CO. In the crystal field model, the energy of the $^1A_{2g}$ state is $10Dq - C$, where $10Dq$ is the usual crystal field splitting and C is the Racah electron repulsion parameter.[59,60] If we take these eigenvalue differences as estimates of $10Dq$ and a value of ~0.3 eV for C, we expect to find $^1A_{2g}$ states in the range 2.6-2.8 eV. The ^1E_g state is estimated to be at 2.3 eV in heme-O_2 and at 2.5 eV in heme-CO.

It is clear that none of the theoretical results is in complete agreement with the assignments of Eaton et al.[5] All of the calculated d→d splittings are too large, although the nonempirical Xα values are only about 0.5 eV higher than experiment; the latter is certainly within the expected limits of error. However, for both carboxy and oxy, the Xα calculation has the ^1E_g level below the $^1A_{2g}$ while, at least for carboxy, the data suggest the reverse order (see above). The EHT results have the $^1A_{2g}$ level below the ^1E_g in both oxy and carboxy with a slightly smaller splitting in the former than the latter (0.25 or 0.45 eV). Also, as already mentioned, the EHT calculation for neither oxy nor carboxy yields a significant lifting of the ^1E_g degeneracy. The same is true for the Xα calculations (see Figures 2 and 3). The PPP results are rather different. In carboxyheme the ^1E_g levels are nearly degenerate and about 0.6 eV below the $^1A_{2g}$ level; in oxy, the ^1E_g splitting is large (0.75 eV) with one of the ^1E_g components below the $^1A_{2g}$ by 0.22 eV and the other above it by 0.55 eV. The large excitation energies obtained from the EHT and PPP models are, of course, due to the particular parametrization. If one accepts the d-d assignments, the parameters chosen for the interaction of the iron 3d and nitrogen σ lone-pair orbitals would have to be reduced. However, there are alternative possibilities for band VI, as discussed above and indicated in Table XII.

D. Intraligand Transitions. The final category of spectral transitions includes those localized on the axial ligand, in this case oxygen. The low-energy state (I) would appear to be one example. The lowest energy promotion we can identify from the Xα molecular orbital diagram is $yz/O_2\pi^* \rightarrow xz/O_2\pi^*$. This is a transition between the two levels whose origins are the degenerate $O_2\pi_g$ orbitals which have been split by the asymmetric binding geometry. Hence this state corresponds roughly to the $^1B_1$ state of ozone. The Xα excitation energy may be estimated from the ground-state MO diagram since the orbitals involved have nearly identical character. This yields an excitation energy of 0.9 eV and makes it a possible candidate for the 0.95-eV absorption.

The lowest $^1A''$ state in the PPP calculation is of the same type. A charge density analysis indicates that 0.10 and 0.82 electrons are transferred from the $3d_{yz}$ and $O_2\pi_g{}^s$ orbitals to $3d_{xz}$ and $O_2\pi_g{}^a$, respectively. For this state the PPP and Xα methods yield the same result. Such a transition should not be present in HbCO since both CO π_g orbitals are unoccupied.

Like band I, band II at 1.1 eV in oxyhemoglobin has a weak absorption with a large CD anisotropy factor. Eaton et al.[5] have assigned this transition to the promotion $d_{x^2-y^2} \rightarrow d_{xz}/O_2\pi_g{}^*$. The X$\alpha$ transition state energy for such a promotion may be estimated from column 4 of Figure 4 to be 2.5 eV. Another possibility is the promotion $d_{yz}/e_g \rightarrow d_{xz}/O_2\pi_g{}^*$ at 2.0 eV. The 2A″ state in the PPP calculation is close to the latter possibility. This state has the form (Table XV)

$$0.707(yz/e_g \rightarrow e_g{}^*/O_2\pi^*) + 0.479(xz/e_g \rightarrow e_g{}^*) + 0.317(yz/e_g \rightarrow \mathrm{Im}/O_2\pi^*) + 0.254(yz/e_g \rightarrow \mathrm{Im}/O_2\pi^*/xz) + \ldots$$

Although the calculated excitation energy (1.7 eV) is larger than the observed value, it is predicted to lie below bands III and IV (see Table XIV). As with the other low-energy transitions, no comparable state is calculated for heme-CO (see Table XV). Finally, band II could be a vibronically excited component of band I. Because of the large discrepancy of calculated and observed energies, it is difficult to draw definite conclusions.

Band VII on oxyhemoglobin is another candidate for an intraligand transition, this time corresponding to the strongly allowed $^1B_2$ excited state of ozone.[8,38] In ozone, this transition

is called the Hartley band and involves π transfer from the central oxygen to the outer atoms. The transition occurs near 4.9 eV in ozone, but is sensitive to geometry.[38,53] No clear-cut assignments can be made from either the Xα or the PPP calculations, although the charge-transfer transitions have been suggested as one possibility (see ref 6 and above). An analogue of the Hartley band would be expected to be intense, but both Xα and PPP place such FeO_2 $\pi \rightarrow \pi^*$ transitions above 5.8 eV. However, in a GVB study of ozone,[38] the excitation energy decreased by 1 eV (5.6 $\rightarrow$ 4.6) upon adding more configurations in a CI treatment. A more careful investigation of this state, perhaps with double CI or with variable geometry, seems warranted.

E. Conclusions. The present set of PPP and Xα calculations, complemented by extended Hückel and ab initio results in the literature, provides a first step toward a unified description of the ground and excited states of the heme group with different ligands. In all of these calculations the complete iron porphine skeleton, as well as two axial ligands, was included. It is clear from the present work that correlation and charge redistribution effects are important for both the ground and excited states of this system. In particular, single-excitation CI is not sufficient for the ground-state energy and for certain transitions in which double excitations play an important role. Nevertheless, a qualitative understanding of some of the excited states can be based on simple one-electron promotions. One difficulty of going beyond this is that it has not proved possible to achieve anything like converged results at the double-excitation level. The Xα method is found to have the advantage over other simple MO schemes of including, through the transition-state procedure, the effects of charge reorganization in the excited states. This effect is of particular importance for charge-transfer transitions, and the Xα method has been successful in describing such transitions in other systems.

Ground-state properties, including the energy and charge distribution, are examined. It is found that correlation effects involving doubly excited configurations must be included to obtain a singlet ground state for the oxygen complex; there is only a small effect from these added configurations on the ground-state charge distribution. The FeO_2 unit is shown to be well represented as an equal mixture of Fe^{2+} ($S = 0$), O_2 ($S = 0$), and Fe^{2+} ($S = 1$), O_2 ($S = 1$) valence-state pairs; the latter resembles ozone in certain respects. The FeCO unit corresponds closely to an idealized Fe^{2+} ($S = 0$), CO ($S = 0$) species. Calculated Mössbauer splittings and infrared stretching frequencies in approximate agreement with the experimental values for both complexes provide support for the present treatment.

In the spectrum of oxy- and carboxyhemoglobin (Tables XII and XIII), a number of points of general agreement between theory and experiment have emerged. The most striking of these is the prediction from three different types of calculation (EH, PPP, and Xα) that an unoccupied FeO_2 π orbital is involved in the low-energy spectrum of heme-O_2; no such low-energy orbital exists in FeCO. As a consequence, in the PPP calculation, for example, there are five states of heme-O_2 below the Q band, and only one (with zero oscillator strength) in the corresponding energy range for heme-CO (see Tables XIV and XV). Our calculations, in agreement with those of Eaton et al.,[5] suggest that bands I and II involve transitions within the FeO_2 unit while bands III and IV represent charge transfer to it from the porphyrin π orbitals. The importance of the porphyrin orbitals for the weak transitions makes it likely that calculations with simplified equatorial ligands[8] cannot be successful in describing such states.

The higher energy transitions are more difficult to interpret. Our calculated d–d transitions are qualitatively in accord with the experimental assignments, but are consistently higher in energy. There are a variety of possibilities for the z-polarized bands VI and VII. The simplest interpretation of our results assigns band VI to the promotion $a_{2u} \rightarrow d_{z^2}$ and band VII to an FeO_2 $\pi \rightarrow \pi^*$ transition.

We hope that, although not unequivocal, the results of the present analysis are sufficient to spur new experimental and theoretical attempts to improve our understanding of the ground and excited states of the heme group in proteins.

Acknowledgments. We thank Iwao Ohmine for advice on the PPP calculations and William A. Eaton for invaluable discussions concerning the spectroscopy of hemoglobins. We also thank Eaton et al. for providing us with the results of their experimental studies and extended Hückel calculations prior to publication. This work was supported by grants from the National Science Foundation and the National Institutes of Health.

Appendix. PPP Parameters

Semiempirical PPP parameters for carbon, nitrogen, and oxygen were obtained from the work of Fischer-Hjalmars and Sundbom,[62] who fitted spectral data for a series of unsaturated hydrocarbons and nitrogen-containing molecules.[63] A method for estimating the values of the iron parameters, which takes into account the charge dependence of the parameters, has been proposed by Blomquist et al.;[21] this method and the parameters were adopted in the present calculation. In the following sections, we will give a brief outline of the approximations used to evaluate the one- and two-electron integrals. We give only values of parameters which have not been included in the references mentioned above.

The two-electron integrals $(\mu\nu|\lambda\sigma)$ are defined by

$$(\mu\nu|\lambda\sigma) = \int\int \phi_\mu^*(1)\phi_\lambda^*(2)(e^2/r_{12})\phi_\nu(1)\phi_\sigma(2)\, d\tau_1\, d\tau_2 \quad \text{(A1)}$$

In calculating these integrals, zero-differential overlap (ZDO) is assumed except for the one-center exchange integrals; that is,

$$(\mu\nu|\lambda\sigma) = \gamma_{\mu\lambda}\delta_{\mu\nu}\delta_{\lambda\sigma} + K_{\mu\lambda}\delta_{\mu\sigma}\delta_{\nu\lambda} + K_{\mu\nu}\delta_{\mu\lambda}\delta_{\nu\sigma} \quad \text{(A2)}$$

where $\gamma_{\mu\nu}$ and $K_{\mu\nu}$ are the Coulomb repulsion and exchange integrals between atomic orbitals ϕ_μ and ϕ_ν; only one-center exchange integrals are included.

For conjugated carbon and nitrogen atoms, $\gamma_{\mu\nu}$ between nearest neighbors is approximated as[62]

$$\gamma_{\mu\nu} = \gamma_{\mu\nu}^0 + \delta_{\mu\nu}^\gamma (R_{\mu\nu} - R^0) \quad \text{(A3)}$$

where $R_{\mu\nu}$ is the distance between the two neighbors, and $\gamma_{\mu\nu}^0$, $\delta_{\mu\nu}^\gamma$, and R^0 are parameters tabulated in ref 62. Other two-center two-electron integrals are approximated by[21]

$$\gamma_{\mu\nu} = \frac{1}{2}(\gamma_{\mu\mu} + \gamma_{\nu\nu}) f(z) \quad \text{(A4)}$$

where

$$z = \frac{1}{2}(\gamma_{\mu\mu} + \gamma_{\nu\nu}) R$$

$$f(z) = (z + e^{-z})^{-1}$$

and R is the distance between the two atoms.

As mentioned in the text (section IIB), the core integral α_μ^i of orbital ϕ_μ, of atom i is approximated by

$$\alpha_\mu^i = \epsilon_\mu^i + \sum_{j \neq i} \langle \mu | V_j | \mu \rangle - \sum_{\substack{\nu \in j \\ j \neq i}} n^\nu \gamma_{\mu\nu} \quad \text{(A5)}$$

where $\epsilon_\mu^i = (\mu | T + V_{\text{core}}^i | \mu)$ represents the interaction between the core of atom i and the electron in the orbital ϕ_μ. Values for the iron orbitals (3d, 4s, and 4p) and for the atomic orbitals of conjugated carbon and nitrogen atoms were taken

Table XVII. PPP Parameters

		Slater exponent	ionization potential, eV
Fe	4s	1.370	−7.90
	4p	1.370	−4.55
	3d	2.722	−8.77
O	2s	2.246	−32.37
	2p	2.227	−13.61
C	2s	1.608	−20.78
	2p	2.227	−9.84
N	2s	1.924	−10.96[a]
	2p	1.917	−10.54[b]

[a] Value for the σ lone pair orbital. [b] Value for the π orbital.

from ref 21. For the ligand oxygen and carbon atoms, they are estimated as follows:

$$\epsilon_{2p}^{O} = I_O(2p) - 2\gamma_{pp'(O)} + K_{pp'(O)} - 2\gamma_{ps(O)} + K_{ps(O)}$$
$$\epsilon_{2s}^{O} = I_O(2s) - \gamma_{ss(O)} - 4\gamma_{ps(O)} + 2K_{ps(O)}$$
$$\epsilon_{2p}^{C} = I_c(2p) - \gamma_{pp'(C)} + \tfrac{1}{2}K_{pp'(C)} - 2\gamma_{ps(C)} + K_{ps(C)} \quad \text{(A6)}$$
$$\epsilon_{2s}^{C} = I_c(2s) - \gamma_{ss(C)} - 2\gamma_{ps(C)} + K_{ps(C)}$$

where O and C represent oxygen and carbon, respectively. The ionization potentials, I, of the valence electrons were taken from atomic data and are listed in Table XVII.

For simplicity, the penetration integrals $\langle\mu|V_j|\mu\rangle$ are neglected except when ϕ_μ is a metal orbital. This metal–ligand penetration integral is assumed to be the same for all iron orbitals and is treated as an adjustable parameter to fit the experimental quadrupole splitting of oxyhemoglobin; the value obtained is 6.78 eV. The effect of including all the penetration integrals is to shift the relative energies of the iron orbitals with respect to those of the ligands. By allowing the metal–ligand penetration integral to vary and by properly choosing the ionization potentials, we expect that an adequate arrangement of the energies of the atomic orbitals can be achieved.

The resonance integrals between the atomic orbitals of conjugated carbon and nitrogen atoms are estimated by[63]

$$\beta_{\mu\nu} = \beta_{\mu\nu}^{0} + \delta_{\mu\nu}^{\beta}(R_{\mu\nu} - R^0) \quad \text{(A7)}$$

where $\beta_{\mu\nu}^{0}$, $\delta_{\mu\nu}^{\beta}$, and R^0 are parameters taken from ref 62. The resonance integrals between iron and its neighboring atoms, and between the atoms of O_2 and CO, are calculated by the formula

$$\beta_{\mu\nu} = \tfrac{1}{2}(k_\mu I_\mu + k_\mu I_\mu)S_{\mu\nu} \quad \text{(A8)}$$

where μ and ν correspond to the atomic orbitals, ϕ_μ and ϕ_ν, I_μ and I_ν are the corresponding ionization potentials, and $S_{\mu\nu}$ is the overlap integral calculated by using the Slater orbitals obtained by Zerner et al.[32] (see Table XVII). The ionization potentials of the iron valence electrons are also taken from ref 30. The constants, k_μ and k_ν, are introduced for the purpose of empirical modification. Following Blomquist et al.,[21] we assumed $k_\mu = k_\nu$ in calculating the resonance integrals between iron and its adjacent nitrogen atoms. To estimate the values of k_{2p} for oxygen, we followed the method described by Fumi and Parr,[64] who calculated the excitation energies of O_2 and fitted the energies to the experimental values of the lowest $^1\Sigma_g^+$, $^1\Delta_g$, and $^3\Sigma^+$ states. We obtain $k_{2p} = 2.260$ and 2.326 for the nuclear distances of 1.208 and 1.297 Å, respectively. Since 1.25 Å is the O–O distance used in the present calculation, the average value 2.29 is adopted for k_{2p}. For the estimation of k_{2s}, we carried out a PPP calculation (with complete single and double CI) on ozone with the same parameters and treated k_{2s} as a variable. By matching the excitation energy of the $1\ ^1B_1$ state to the Chappuis band (2.03–2.25 eV, maxima at 2.06 and 2.16 eV), we obtain a value of 1.429 for k_{2s}. For the carbon atomic orbitals, the values of k_{2p} is assumed to be 1.968 from the CNDO parameters,[65] and the value of k_{2s} is assumed to be 1.0. All of these k values are to be regarded as empirical fitting parameters and no attempt has been made to interpret them theoretically.

References and Notes

(1) (a) Department of Chemistry, University of California, Davis, Calif. 95616. (b) Freshwater Biological Institute, University of Minnesota, Navarre, Minn. 55392.
(2) B. H. Huynh, D. A. Case, and M. Karplus, *J. Am. Chem. Soc.*, **99**, 6103 (1977).
(3) G. Lang and W. Marshall, *Proc. Phys. Soc., London*, **87**, 3 (1966).
(4) J. P. Collman, J. I. Brauman, T. G. Halbert, and K. S. Suslick, *Proc. Natl. Acad. Sci. U.S.A.*, **73**, 3333 (1976), and references cited therein.
(5) W. A. Eaton, L. K. Hanson, P. J. Stephens, J. C. Sutherland, and J. B. R. Dunn, *J. Am. Chem. Soc.*, **100**, 4991 (1978).
(6) A. K. Churg and M. W. Makinen, *J. Chem. Phys.*, **68**, 1913 (1978); it should be noted that the *x* and *y* axes are interchanged in this reference, relative to the ones used in ref 5 and in the present paper.
(7) L. Pauling, *Nature (London)*, **203**, 182 (1964); *Stanford Med. Bull.*, **6**, 215 (1948).
(8) W. A. Goddard, III, and B. D. Olafson, *Proc. Natl. Acad. Sci. U.S.A.*, **72**, 2335 (1975); D. B. Olafson and W. A. Goddard, III, *ibid.*, **74**, 1315 (1977).
(9) J. J. Weiss, *Nature (London)*, **202**, 83 (1964).
(10) For example, see M. F. Perutz, J. V. Kilmartin, K. Nagai, A. Szabo, and S. R. Simon, *Biochemistry*, **15**, 378 (1976), and references cited therein.
(11) E. Antonini and M. Brunori, "Hemoglobin and Myoglobin in Their Reactions with Ligands", North-Holland Publishing Co., Amsterdam, 1971.
(12) M. W. Makinen and W. A. Eaton, *Ann. N.Y. Acad. Sci.*, **206**, 210 (1973).
(13) J. P. Collman, R. P. Gagne, C. A. Reed, W. T. Robinson, and G. A. Rodley, *Proc. Natl. Acad. Sci. U.S.A.*, **71**, 1326 (1976).
(14) S. E. V. Phillips, *Nature (London)*, **273**, 247 (1978).
(15) S. M. Peng and J. A. Ibers, *J. Am. Chem. Soc.*, **98**, 8032 (1976).
(16) J. C. Norvell, A. C. Nunes, and B. P. Schoenborn, *Science*, **190**, 568 (1975).
(17) E. J. Heidner, R. C. Ladner, and M. F. Perutz, *J. Mol. Biol.*, **104**, 707 (1976).
(18) D. A. Case and M. Karplus, *J. Mol. Biol.*, **123**, 697 (1978).
(19) P. Eisenberger, R. G. Shulman, G. S. Brown, and S. Ogawa, *Proc. Natl. Acad. Sci. U.S.A.*, **73**, 491 (1976); P. Eisenberger, R. G. Shulman, B. M. Kincaid, G. S. Brown, and S. Ogawa, *Nature (London)*, **274**, 30 (1978).
(20) H. Kobayashi, *J. Chem. Phys.*, **30**, 1362, 1373 (1959); C. Weiss, H. Kobayashi, and M. Gouterman, *J. Mol. Spectrosc.*, **16**, 415 (1965).
(21) J. Blomquist, B. Norden, and M. Sundbom, *Theor. Chim. Acta*, **28**, 313 (1973), and references cited therein.
(22) M. Goeppert-Mayer and A. Sklar, *J. Chem. Phys.*, **6**, 645 (1938).
(23) I. Shavitt in "Modern Quantum Chemistry", Vol. II, G. A. Segal, Ed., Plenum Press, New York, 1976.
(24) K. H. Johnson, *Adv. Quantum Chem.*, **7**, 143 (1973); *Annu. Rev. Phys. Chem.*, **26**, 39 (1975).
(25) J. W. D. Connolly in "Modern Theoretical Chemistry", Vol. IV, G. A. Segal, Ed., Plenum Press, New York, 1976.
(26) D. A. Case and M. Karplus, *J. Am. Chem. Soc.*, **99**, 6182 (1977).
(27) J. G. Norman, Jr., *J. Am. Chem. Soc.*, **96**, 3327 (1974); *J. Chem. Phys.*, **61**, 4630 (1974); *Mol. Phys.*, **31**, 1191 (1976).
(28) J. B. Johnson and W. G. Klemperer, *J. Am. Chem. Soc.*, **99**, 7132 (1977).
(29) D. R. Salahub, R. P. Messmer, and K. H. Johnson, *Mol. Phys.*, **31**, 529 (1976).
(30) D. A. Case and M. Karplus, *Chem. Phys. Lett.*, **39**, 33 (1976).
(31) N. H. F. Beebe, *Chem. Phys. Lett.*, **19**, 290 (1973).
(32) M. Zerner, M. Gouterman, and H. Kobayashi, *Theor. Chim. Acta*, **6**, 363 (1966); M. Zerner and M. Gouterman, *ibid.*, **4**, 44 (1966).
(33) R. F. Kirchner and G. H. Loew, *J. Am. Chem. Soc.*, **99**, 4639 (1977); S. Aronowitz, M. Gouterman, and J. C. W. Chien, *Theor. Chim. Acta*, to be published.
(34) S. J. Chantrell, C. A. McAuliffe, R. W. Munn, and A. C. Pratt, *Coord. Chem. Rev.*, **16**, 259 (1975).
(35) A. Dedieu, M.-M. Rohmer, and A. Viellard in "Metal Ligand Interactions in Organic Chemistry and Biochemistry", Proceedings of the 9th Jerusalem Symposium on Quantum Chemistry and Biochemistry, March 29–April 2, 1976; A. Dedieu, M.-M. Rohmer, M. Bernard, and A. Veillard, *J. Am. Chem. Soc.*, **98**, 3717 (1976); A. Dedieu, M.-M. Rohmer, H. Veillard, and A. Veillard, *Bull. Soc. Chim. Belg.*, **85**, 953 (1976).
(36) D. A. Case, Ph.D. Thesis, Harvard University, 1977, Chapter 6.
(37) H. Kuhn, *J. Chem. Phys.*, **17**, 1198 (1949); W. T. Simpson, *ibid.*, **17**, 1218 (1949); J. R. Platt, *ibid.*, **22**, 1448 (1954).
(38) P. J. Hay, T. H. Dunning, Jr., and W. A. Goddard, III, *J. Chem. Phys.*, **62**, 3912 (1975).
(39) A. Dedieu, M.-M. Rohmer, and A. Veillard, *J. Am. Chem. Soc.*, **98**, 5789 (1976).
(40) M. F. Perutz, *Proc. R. Soc. London, Ser. B*, **173**, 113 (1969).
(41) Y. Seno, J. Otsuka, O. Matsuoka, and N. Fuckikami, *J. Phys. Soc. Jpn.*, **33**, 1645 (1972); **35**, 854 (1973); **41**, 977 (1976).
(42) J. C. Maxwell, J. A. Volpe, C. H. Barlow, and W. S. Caughey, *Biochem. Biophys. Res. Commun.*, **58**, 166 (1974); C. H. Barlow, J. C. Maxwell, W. J. Wallace, and W. S. Caughey, *ibid.*, **55**, 91 (1973).
(43) W. S. Caughey, *Ann. N.Y. Acad. Sci.*, **174**, 148 (1970).
(44) A. Trautwein, *Struct. Bonding (Berlin)*, **20**, 101 (1974); Y. Maeda, T. Marami, Y. Morita, A. Trautwein, and V. Gonser, *J. Phys. (Paris)*, in press; F. Parak, V. F. Thomanek, D. Bade, and B. Wintergerst, *Z. Naturforsch. C*, **32**, 507 (1977).

(45) U. Gonser, Y. Maeda, A. Trautwein, F. Parah, and H. Formanek, *Z. Naturforsch.*, **296**, 241 (1974).
(46) L. Marchant, M. Sharrock, B. M. Hoffman, and E. Munck, *Proc. Natl. Acad. Sci. U.S.A.*, **69**, 2396 (1972).
(47) K. Spartalian, G. Lang, J. P. Collman, R. R. Gagne, and C. A. Reed, *J. Chem. Phys.*, **63**, 5375 (1975).
(48) M. Weissbluth, *Struct. Bonding (Berlin)*, **2**, 1 (1967).
(49) J. Blomquist, A. Henriksson-Enflo, and M. Sundbom, University of Stockholm Institute of Physics Report, April 1974.
(50) M. Cerdonio, A. Congiu-Castellano, F. Mongo, B. Pispisa, G. L. Romani, and S. Vitale, *Proc. Natl. Acad. Sci. U.S.A.*, **74**, 398 (1977).
(51) L. Pauling, *Proc. Natl. Acad. Sci. U.S.A.*, **74**, 2612 (1977).
(52) R. H. Austin, K. Beeson, L. Eisenstein, H. Frauenfelder, and I. C. Gunsalus, *Biochemistry*, **14**, 5355 (1975).
(53) D. Grimbert and A. Devaquet, *Mol. Phys.*, **27**, 831 (1974).
(54) W. A. Eaton and R. M. Hochstrasser, *J. Chem. Phys.*, **46**, 2533 (1967); **49**, 985 (1968).
(55) K. Schulten, I. Ohmine, and M. Karplus, *J. Chem. Phys.*, **64**, 4422 (1976).
(56) B. Roos and M. Sundbom, *J. Mol. Spectrosc.*, **36**, 8 (1970).
(57) J. B. W. Wittenberg, B. A. Wittenberg, J. Peisach, and W. E. Blumberg, *Proc. Natl. Acad. Sci. U.S.A.*, **67**, 1846 (1970).
(58) J. M. Baldwin, private communication.
(59) J. Harris and R. O. Jones, *J. Chem. Phys.*, **68**, 3316 (1978).
(60) W. A. Eaton and E. Charney, *J. Chem. Phys.*, **51**, 4502 (1969); in "Probes of Structure and Function in Macromolecules and Membranes", Vol. I, B. Chance, C. P. Lee, and J. K. Blasie, Eds., Academic Press, New York, 1971, p 155.
(61) W. Moffitt, *J. Chem. Phys.*, **25**, 1189 (1956); C. J. Ballhausen and W. Moffitt, *J. Inorg. Nucl. Chem.*, **3**, 178 (1956).
(62) I. Fischer-Hjalmars and M. Sundbom, *Acta Chem. Scand.*, **22**, 607 (1968).
(63) M. Sundbom, *Acta. Chem. Scand.*, **25**, 487 (1971).
(64) F. G. Fumi and R. G. Parr, *J. Chem. Phys.*, **21**, 1864 (1953).
(65) J. A. Pople and D. L. Beveridge, "Approximate Molecular Orbital Theory", McGraw-Hill, New York, 1970.

On the Effects of Methyl Substitution on the Excited States of Butadiene

U. Dinur[1a,b] and B. Honig*[1a,c]

Contribution from the Department of Physical Chemistry, The Hebrew University, Jerusalem, Israel. *Received June 19, 1978*

Abstract: The effects of methyl substitution on the excited-state properties of butadiene are studied. Hyperconjugation and inductive effects are considered in detail and it is shown that the semiempirical parametrization normally used to account for the latter may be justified on the basis of ab initio calculations. The spectroscopic red shift resulting from methyl substitution in butadiene has two origins. In 1-methylbutadiene it is due to hyperconjugation while in 2-methylbutadiene inductive mixing between the optically forbidden A_g^- state and the allowed B_u^+ state is found to be important. The description of these effects within the framework of MO theory requires that doubly excited configurations be included in the CI scheme; however, they are intuitively obvious from consideration of valence bond structures. Charge distributions are strongly affected by the inclusion of doubly excited configurations and the A_g^- and B_u^+ states are found to have reverse directions of polarization. The CNDO/S method is shown to be incapable of properly treating inductive effects and may be replaced, for the compounds under consideration, by a π electron scheme in which the π orbitals of the methyl group have been appropriately parametrized.

Introduction

Methyl substitution in conjugated molecules has pronounced effects on absorption spectra. These often arise from conformational changes induced by steric hindrance[2] as is the case, for example, in retinals, the chromophore of the visual pigments.[3] In addition, there are always intrinsic changes in electronic structure leading generally to 5–10-nm red shifts per methyl group (Woodward's rules[4]). Synthetically modified retinals where methyl groups have been added or deleted have been used extensively in visual pigment research and large spectroscopic and photochemical effects have been observed.[5] Our interest in understanding these effects has led us to consider the modifications in the excited-state properties of polyenes that result from methyl substitution.

Theoretical studies of methylation in olefins have been primarily concerned with ground-state properties and have been based both on semiempirical and ab initio calculations employing single determinental wave functions.[6-8] Using propene and methylacetylene as prototypes it was found, for example, that in the absence of steric hindrance the main effect of methylation is the polarization of the π molecular orbitals of the chromophore such that substituted positions lose electron density.[6-8]

In the present paper we take *trans*-butadiene as a prototype of linear polyenes and discuss charge distributions and spectral shifts in its methylated derivatives. Some spectroscopic effects can be understood in terms of ground-state properties while in others a detailed description of excited states is required. Of particular interest is the influence of doubly excited configurations on the calculated quantities. Attempts to account for the spectroscopic effects of methyl substitution have been reported previously.[9-11] However, no general agreement seems to exist as to the relative importance of the inductive and hyperconjugation effects and this question and the related consequences of double excitations are treated here in some detail.

The main absorption band in essentially all polyenes corresponds to a transition from the ground state to an excited state of B_u^+ symmetry. This state has generally been considered to be the lowest singlet; however, recent experimental studies on a number of polyenes have revealed a weakly allowed transition at longer wavelengths than the main band[12] (see also below). π electron calculations which include doubly excited configurations in the CI scheme predict the existence of a state of A_g^- symmetry below the B_u^+ state[13] (although calculations using only single excitations place the A_g^- state at significantly higher energies). Thus there seems to be excellent agreement between theory and experiment for the longer polyenes.

The situation for the shorter polyenes such as butadiene is less clear since no absorption band at longer wavelengths than the main transition has been detected experimentally.[41] However, π electron calculations on butadiene indicate that the A_g^- state is still below the B_u^+ with a small energy difference separating the two states.[13] A number of extensive ab initio calculations have also been carried out on butadiene.[14]

0002-7863/79/1501-4453$01.00/0